European Journal of Pharmaceutical Sciences 55 (2014) 20–35

Contents lists available at ScienceDirect

European Journal of Pharmaceutical Sciences

journal homepage: www.elsevier.com/locate/ejps

# Synthesis and toxicological studies of *in vivo* anticoagulant activity of novel 3-(1-aminoethylidene)chroman-2,4-diones and 4-hydroxy-3-(1-iminoethyl)-*2H*-chromen-2-ones combined with a structure-based 3-D pharmacophore model

Nevena Stanković [a,*], Milan Mladenović [a], Mirjana Mihailović [b], Jelena Arambašić [b], Aleksandra Uskoković [b], Vesna Stanković [c], Vladimir Mihailović [a], Jelena Katanić [a], Sanja Matić [d], Slavica Solujić [a], Nenad Vuković [a], Slobodan Sukdolak [a]

[a] *Kragujevac Center for Computational Biochemistry, Department of Chemistry, Faculty of Science, University of Kragujevac, Radoja Domanovića 12, P.O. Box 60, 34000 Kragujevac, Serbia*
[b] *Department of Molecular Biology, Institute for Biological Research, University of Belgrade, Bulevar Despota Stefana 142, 11000 Belgrade, Serbia*
[c] *Institute of Pathology, Faculty of Medical Sciences, Svetozara Markovića 69, P.O. Box 60, 34000 Kragujevac, Serbia*
[d] *Department of Biology and Ecology, Faculty of Science, University of Kragujevac, Radoja Domanovića 12, P.O. Box 60, 34000 Kragujevac, Serbia*

ARTICLE INFO

*Article history:*
Received 29 July 2013
Received in revised form 13 January 2014
Accepted 15 January 2014
Available online 24 January 2014

*Keywords:*
Chroman-2,4-diones
Anticoagulant activity *in vivo*
Histopathology
Molecular docking
3-D pharmacophore

ABSTRACT

Eight synthesized 3-(1-aminoethylidene)chroman-2,4-diones and 4-hydroxy-3-(1-iminoethyl)-*2H*-chromen-2-ones were evaluated as *in vivo* anticoagulants by *intraperitoneal* application to adult male Wistar rats in order to examine their pharmacological potential, evaluate ther toxicity and propose the mechanism of action. Two of them, **2f** and **2a**, in concentration of 2 mg/kg of body weight, presented remarkable activity (PT = 130 s; PT = 90 s) upon seven days of continuous application. The results of rat serum and liver biochemical screening, as well those of histopathological studies, proved the compounds to be non-toxic. Activity of the compounds was further examined on the molecular level. Here, molecular docking studies were performed to position the compounds in relation to the active site of VKORC1 and determine the bioactive conformations. Docking results suggested a non-covalent mode of action during which the proton transfer occurs from Cys135 SH towards 4-carbonyl group of anticoagulant. All crucial interactions for anticoagulant activity were confirmed in generated structure-based 3-D pharmacophore model, consisted of hydrogen bond acceptor and hydrophobic aromatic features, and quantified by a best correlation coefficient of 0.97.



## 1. Introduction

Among all well documented biological activities of coumarin compounds (Rodríguez et al., 2011; Satyanarayan et al., 2008; Karali et al., 2002; Natala et al., 2004), the anticoagulant activity of 4-hydroxycoumarins and related derivatives is of the greatest importance (Au and Rettie, 2008). As anticoagulants, 4-hydroxycoumarins act as competitive inhibitors of vitamin K-2,3-epoxide reductase subunit 1 (VKORC1), a liver endoplasmic reticulum protein with transmembrane topology (Oldenburg et al., 2007). They prevent the reduction of vitamin K-2,3-epoxide, which is formed at the end of the coagulation cycle, to vitamin K hydroquinone, which begins the new cycle. Consequently, vitamin K-dependent synthesis of biologically active forms of clotting factors II (prothrombin), VII, IX, and X is temporarily blocked (Ridker et al., 2003). With the inhibition of prothrombin production there is a delay in the formation of thrombin from prothrombin known as prothrombin time, which is used as a measure of the ability of an anticoagulant to prolong the formation of blood clot. Patients suffering from venous thrombosis, pulmonary embolism, or heart attack (Hirch et al., 2003) benefit from taking oral anticoagulants like warfarin. The treatment with anticoagulants includes continuous administration of compounds and constant monitoring of prothrombin time (Jaffer and Bragg, 2003).

Drugs like warfarin are transferred to the active site of VKORC1 by serum albumin in the open side chain form (Petitpas et al., 2001). Since there is still no available co-crystallized structure of

* Corresponding author. Tel.: +381 34336223; fax: +381 34335040.
*E-mail address:* nevenas@kg.ac.rs (N. Stanković).

http://dx.doi.org/10.1016/j.ejps.2014.01.004
0928-0987/

the warfarin–VKORC1 complex, the active form of the drug during anticoagulant activity is so far unknown. To perform inhibition of the coagulation cycle, it is believed that warfarin (or any 4-hydroxycoumarin structure, in general) must be transformed into the deprotonated open side chain form (Karlsson et al., 2007; Henschel et al., 2010), i.e., the chroman-2,4-quinone form, in which the drug shares structural similarities with vitamin K-2,3-epoxide and acts as a competitive inhibitor. The formation of a chroman-2,4-quinone represents the crucial moment in the prolongation of clotting. Based on what is known so far, two steps are involved in the anticoagulant activity of warfarin. The first is binding of the side chain 3-(3-oxo-1-phenylbutyl) functional group to amino acids Thr138, Tyr139, and Ala140 in the VKORC1 active site (Oldenburg et al., 2007). The second step is interaction between the 4-carbonyl oxygen of the newly formed chroman-2,4-quinone and the catalytic center amino acids Cys132–Cys135 (Oldenburg et al., 2007). On the basis of recent molecular docking and DFT mechanistic studies, it was proposed that the SH group of Cys135 interacts with carbonyl oxygen, which results in proton transfer from the amino acid side chain to the chroman-2,4-quinone (Mladenović et al., 2012). The reaction ends when a coumarin 4-hydroxyl group and disulfide bond are formed (Oldenburg et al., 2007). Apart from the fact that the biochemical mechanism of warfarin's anticoagulant activity is essentially oxido-reduction, it is known that the reaction occurs on the enzyme itself without any cofactor (Deerfield et al., 2006).

Despite of the long-established clinical usage of warfarin and related drugs as anticoagulants, unfavorable side effects like induced internal hemorrhage (Fang et al., 2011) or bone damage (Sugiyama et al., 2007) are well documented. There is a need therefore to discover new highly potent chroman-2,4-quinone and 4-hydroxycoumarin anticoagulants which will present no undesirable effects. The above mentioned study (Mladenović et al., 2012) showed that 4-hydroxycoumarins which bear polar C-3 substituents and are therefore structurally different from warfarin in a low dose can exhibit significant *in vivo* anticoagulant activity. In the light of that discovery, the present paper summarizes efforts to evaluate eight novel chroman-2,4-diones and 4-hydroxy-*2H*-chromen-2-ones hitherto untested as *in vivo* anticoagulants. Chroman-2,4-diones (chroman-2,4-quinones) are usually cited as a sub-class of 4-hydroxycoumarins, since they are products of 4-hydroxyl group intramolecular tautomerisation (Khoobi et al., 2011). Anticoagulant activity was evaluated by measuring the prothrombin time after the application to adult male Wistar rats. Afterwards, chemically induced hepatic toxicity was determined by measuring the values of various biochemical markers and by performing histopathological evaluation. In order to understand *in vivo* activity on the molecular level, molecular docking studies were performed on an in-house constructed homology model of rat VKORC1 (Mladenović et al., 2012). Monitoring of *in vivo* activity was accompanied by construction of a structure-based 3-D pharmacophore model that explained it in great detail.

## 2. Materials and methods

### 2.1. General

For the preparation of compounds, two synthetic procedures were used: conventional and microwave-assisted. All reagents and solvents were of analytical grade and used directly. All melting points of the synthesized compounds were recorded on a Kofler hot-stage apparatus (C. Reichert, Vienna, Austria) and uncorrected. Microwave-assisted reactions were carried out in a MICROSYNTH Microwave Synthesis System (serial number: 130486, terminal: T640, serial number: 0804000100), manufactured by Milestone Inc. 25 Controls Dr. Shelton, CT 06484, USA. The microwaves were generated by a magnetron (serial number: 133462/13346) at a frequency of 2450 MHz, having an output energy range of 100–500 W. The purity of obtained compounds was checked routinely by TLC using Merck Kieselgel 60 $PF_{254+366}$ and Merck Kieselgel G. The TLC spots were visualized by exposing the dry plates in iodine vapors. Purity was also checked by gas-chromatography/mass spectrometry. Microanalysis of carbon, hydrogen, nitrogen, and sulfur was carried out with a Carlo Erba 1106 microanalyzer (Carlo Erba, Milan, Italy). The IR spectra were recorded on a Perkin–Elmer grating spectrophotometers Model 137 and Model 337, in $cm^{-1}$ (Perkin Elmer, Beaconsfield, UK). The NMR spectra were recorded on a Varian Gemini 200 spectrometer ($^1H$ at 200 MHz; $^{13}C$ at 50 MHz; Varian Inc., Palo Alto, CA, USA) in DMSO as solvent using TMS ($SiMe_4$) as the internal standard. Chemical shifts are given in ppm (abbreviations: s-singlet, d-doublet, t-triplet, q-quartet, ABq-AB quartet, m-multiplet). GC/MS analyses were carried out in an Agilent 6890N/5975B gas chromatograph. All NMR spectral data are supplied in Supplementary information, Figs. S6–S22.

### 2.2. General procedure for preparation of chroman-2,4-dione and 4-hydroxy-2H-chromen-2-one derivatives

#### 2.2.1. Conventional synthesis

*2.2.1.1. (E)-3-(1-(2-aminoethylamino)ethylidene)chroman-2,4-dione (**2a**).* To a mixture of ethylenediamine hydrochloride (0.326 g, 2.45 mmol) and $Et_3N$ (0.248 g, 2.45 mmol) in 50 mL of MeOH, 3-acetyl-4-hydroxycoumarin (**1**) (0.5 g, 2.45 mmol) was added partially. Synthesis of 3-acethyl-4-hydroxycoumarin was described elsewhere (Sukdolak et al., 2005). The reaction solution was mixed with magnetic stirrer at room temperature for 30 min. After completion of the reaction, the reaction mixture was evaporated under reduced pressure to a third of the volume and **2a** was filtered and re-crystallized from methanol. White crystals, yield: 94%, mp: 163.5–164.0 °C. IR (KBr): $\upsilon_{max}$ $cm^{-1}$ 3414, 3139, 3012, 2948, 2805, 1671, 1609, 1563, 1504, 1462; $^1H$ NMR (200 MHz, DMSO-$d_6$): $\delta$ ppm 11.08 (br s, 1H, NH), 8.36–7.55 (m, 4H, C—H-5, C—H-6, C—H-7, C—H-8), 3.40 (br s, 2H, $NH_2$), 3.21 (t, 2H, $CH_2$—C, $^3J_{HH}$ = 9.4 Hz), 2.97 (t, $CH_2$, $CH_2$—C, $^3J_{HH}$ = 9.4 Hz), 2.62 (s, 3H, $CH_3$—C). $^{13}C$ NMR (50 MHz, DMSO): $\delta$ ppm 183.66, 176.82, 163.60, 154.23, 133.60, 126.26, 124.56, 121.72, 118.40, 100.30, 60.60, 45.62, 18.26. MS: *m*/*z* 246 ($M^+$), 247 ($M^+$+1). Anal. calcd. (%) for $C_{13}H_{14}N_2O_3$: C, 63.40; H, 5.73; N, 11.38; Found: C, 61.56; H, 5.48; N, 11.02.

*2.2.1.2. (E)-3-(1-(2-hydroxyethylamino)ethylidene)chroman-2,4-dione (**2b**).* To a mixture of 2-aminoethanol (0.149 g, 2.45 mmol) and $Et_3N$ (0.248 g, 2.45 mmol) in 50 mL of MeOH, 3-acetyl-4-hydroxycoumarin (**1**) (0.5 g, 2.45 mmol) was added fractionally and reaction mixture was refluxed for 2 h. The solvent was then evaporated under reduced pressure to a third of the volume and left standing at 5 °C for 24 h. Afterwards, the precipitated white compound **2b** was collected by filtration and re-crystallized from methanol. White crystals, yield: 97%, mp: 157.2–159.4 °C. IR (KBr): $\upsilon_{max}$ $cm^{-1}$ 3550–3200, 3412, 3050, 2948, 2894, 1661, 1615, 1592, 1573, 1487. $^1H$ NMR (200 MHz, DMSO-$d_6$): $\delta$ ppm 14.00 (br s, 1H, NH), 8.36–7.55 (m, 4H, C—H-5, C—H-6, C—H-7, C—H-8), 4.48 (br s, 1H, OH), 3.61 (t, 2H, $CH_2$—O, $^3J_{HH}$ = 8.4 Hz), 3.48 (t, 2H, $CH_2$—C, $^3J_{HH}$ = 7.9 Hz), 2.62 (s, 3H, $CH_3$—C). $^{13}C$ NMR (50 MHz, DMSO): $\delta$ ppm 183.06, 176.82, 163.60, 154.23, 133.60, 126.26, 124.56, 121.72, 118.40, 100.30, 60.60, 45.62, 18.24. MS: *m*/*z* 281 ($M^+$). Anal. calcd. (%) for $C_{13}H_{13}NO_4$: C, 63.15; H, 5.30; N, 5.67. Found: C, 62.78; H, 5.10; N, 5.87.

*2.2.1.3. (E)-3-(1-(2-mercaptoethylamino)ethylidene)chroman-2,4-dione (**2c**).* To a mixture of 2-mercaptoethanolamine hydrochloride

(0.189 g, 2.45 mmol) and $Et_3N$ (0.248 g, 2.45 mmol) in 50 mL of MeOH, 3-acetyl-4-hydroxycoumarin (**1**) (0.5 g, 2.45 mmol) was added fractionally and the reaction mixture was refluxed for 2 h. After 30 min of reflux, the appearance of a white precipitate was observed. The solvent was than evaporated under reduced pressure to a third of the volume and left standing at 5 °C for 24 h. Afterwards, the precipitated white compound **2c** was collected by filtration and re-crystallized from methanol. White crystals, yield: 86%, mp: 172–174 °C. IR (KBr): $\upsilon_{max}$ $cm^{-1}$ 3414, 3051, 3015, 2973, 2782, 2530, 1687, 1607, 1574, 1483. $^1H$ NMR (200 MHz, DMSO-$d_6$): $\delta$ ppm 11.08 (br s, 1H, NH), 8.37–7.55 (m, 4H, C—H-5, C—H-6, C—H-7, C—H-8), 3.40 (m, 2H, $CH_2$—C, $^3J_{HH}$ = 8.1 Hz), 3.18 (m, 2H, $CH_2$—C), 2.62 (s, 3H, $CH_3$—C), 1.40 (br s, 1H, SH). $^{13}C$ NMR (50 MHz, DMSO): $\delta$ ppm 183.06, 176.82, 163.60, 154.23, 133.60, 126.26, 124.56, 121.72, 118.40, 100.30, 42.40, 29.42, 18.26. MS: *m*/*z* 265 ($M^+$+2), 263 ($M^+$+1). Anal. calcd. (%) for $C_{13}H_{13}NO_3S$: C, 59.30; H, 4.98; N, 5.32. Found: C, 59.21; H, 5.07; N, 5.35.

*2.2.1.4. (E)-3-(1-(2-(methylamino)ethylamino)ethylidene)chroman-2,4-dione (**2d**).* Minor modifications of the conventional procedure were performed in order to obtain compound **2d** in crystalline state. Thus, 3-acetyl-4-hydroxycoumarin (**1**) (0.5 g, 2.45 mmol) was added to 25 mL of heated MeOH solution. The solution was cooled to room temperature, after which 10 mL of MeOH containing $N^1$-methylethane-1,2-diamine (0.182 g, 2.45 mmol) was added. The mixture was heated for 10 more min until the initial color of the coumarin compound disappeared. The solvent was then evaporated under reduced pressure to a third of the initial volume and left standing at 5 °C for 24 h. Afterwards, the precipitated yellow compound **2d** was collected by filtration and re-crystallized from methanol. White crystals, yield: 82%, mp: 180–182 °C. IR (KBr): $\upsilon_{max}$ $cm^{-1}$ 3412, 3308, 3051, 3017, 2923, 1663, 1614, 1573, 1524, 1484. $^1H$ NMR (200 MHz, DMSO-$d_6$): $\delta$ ppm 11.08 (br s, 1H, NH), 8.36–7.55 (m, 4H, C—H-5, C—H-6, C—H-7, C—H-8), 3.29 (t, 2H, $CH_2$—C, $^3J_{HH}$ = 8.9 Hz), 2.66 (t, 2H, $CH_2$—C, $^3J_{HH}$ = 8.9 Hz), 2.62 (s, 3H, $CH_3$—C), 2.40 (br s, 1H, NH—$CH_3$), 2.29 (s, 3H, $CH_3$—N). $^{13}C$ NMR (50 MHz, DMSO): $\delta$ ppm 183.06, 176.82, 163.60, 154.23, 133.60, 126.26, 124.58, 121.72, 118.40, 100.30, 50.73, 43.11, 36.30, 18.26. MS: *m*/*z* 260 ($M^+$). Anal. calcd. (%) for $C_{14}H_{16}N_2O_3$: C, 64.60; H, 6.20; N, 10.76. Found: C, 64.66; H, 6.11; N, 11.16.

*2.2.1.5. (3E,3′E)-3,3′-(1,1′-(propane-1,3-diylbis(azanediyl))bis(ethan-1-yl-ylidene))dichroman-2,4-dione (**2e**).* To a mixture of 1,3-diaminopropane hydrochloride (0.182 g, 2.45 mmol) and $Et_3N$ (0.496 g, 4.50 mmol) in 50 mL of MeOH, 3-acetyl-4-hydroxycoumarin (0.5 g, 2.45 mmol) was added fractionally. The reaction mixture was refluxed for 30 min, during which the appearance of a white precipitate was observed. White solid, yield: 41%, mp: 243–246 °C. IR (KBr): $\upsilon_{max}$ $cm^{-1}$ 3420, 3037, 2936, 2871, 2873, 1707, 1608, 1572, 1485, 1467. $^1H$ NMR (200 MHz, DMSO-$d_6$): $\delta$ ppm 11.08 (br s, 1H, NH), 8.28–7.48 (m, 4H, C—H-5, C—H-6, C—H-7, C—H-8), 3.23 (t, 2H, $CH_2$—C, $^3J_{HH}$ = 9.4 Hz), 3.08 (t, $CH_2$, $CH_2$—C, $^3J_{HH}$ = 9.4 Hz), 1.51 (s, 3H, $CH_3$—C). $^{13}C$ NMR (50 MHz, DMSO): $\delta$ ppm 183.06, 176.82, 163.60, 154.23, 133.60, 126.26, 124.56, 121.72, 118.40, 100.30, 41.24, 28.55, 18.26. MS: *m*/*z* 446 ($M^+$), 447 ($M^+$+1), 448 ($M^+$+2). Anal. calcd. (%) for $C_{25}H_{22}N_2O_6$: C, 67.26; H, 4.97; N, 6.27. Found: C, 67.56; H, 4.33; N, 6.97.

*2.2.1.6. (3E,3′E)-3,3′-(1,1′-(ethane-1,2-diylbis(azanediyl))bis(ethan-1-yl-1-ylidene))dichroman-2,4-dione (**2f**).* To a mixture of ethylenediamine hydrochloride (0.326 g, 2.45 mmol) and $Et_3N$ (0.496 g, 4.50 mmol) in 50 mL of MeOH, 3-acetyl-4-hydroxycoumarin (0.5 g, 2.45 mmol) was added fractionally. The reaction mixture was refluxed for 30 min, during which the appearance of a white precipitate was observed. White solid, yield: 47%, mp: 238–241 °C. IR (KBr): $\upsilon_{max}$ $cm^{-1}$ 3414, 3050, 3015, 2923, 2853, 1699, 1609, 1571, 1486, 1466. $^1H$ NMR (200 MHz, DMSO-$d_6$): $\delta$ ppm 11.08 (br s, 1H, NH), 8.21–7.39 (m, 4H, C—H-5, C—H-6, C—H-7, C—H-8), 3.27 (m, 2H, $CH_2$—C, $^3J_{HH}$ = 9.4 Hz), 3.11 (s, 3H, $CH_3$—C). $^{13}C$ NMR (50 MHz, DMSO): $\delta$ ppm 183.06, 175.82, 163.60, 154.23, 133.60, 126.26, 124.56, 121.72, 118.40, 100.30, 43.99, 18.26. MS: *m*/*z* 432 ($M^+$), 433 ($M^+$+1), 434 ($M^+$+2). Anal. calcd. (%) for $C_{24}H_{20}N_2O_6$: C, 66.66; H, 4.66; N, 6.48. Found: C, 66.87; H, 4.31; N, 6.52.

*2.2.2. Microwave-assisted synthesis*

*2.2.2.1. N-[(1E)-1-(4-hydroxy-2-oxo-2H-chromen-3-yl)ethylidene]aminosulfonamide (**2g**).* An equimolar amount of sulfamide was added to a 50 mL methanol solution of 3-acetyl-4-hydroxychromene-2-one (**1**) (0.5 g, 2.45 mmol). The mixture was heated under microwaves for 10 min. After cooling, the solvent was removed and the obtained solid filtered and re-crystallized from methanol. Yellow crystals, yield: 76%, mp: 189–191 °C. IR (KBr): $\upsilon_{max}$ $cm^{-1}$ 3423, 3132, 3054, 3018, 2928, 2856, 1699, 1674, 1611, 1579, 1484, 1466, 1386, 1131, 698. $^1H$ NMR (200 MHz, DMSO-$d_6$): $\delta$ ppm 13.86 (br s, 1H, OH), 7.87–6.96 (m, 4H, C—H-5, C—H-6, C—H-7, C—H-8), 4.32 (br s, 2H, S-$NH_2$), 2.38 (s, 3H, $CH_3$—C). $^{13}C$ NMR (50 MHz, DMSO): $\delta$ ppm 174.68, 173.42, 161.64, 153.37, 132.23, 124.69, 123.84, 116.46, 115.77, 100.65, 17.86. MS: *m*/*z* 282 ($M^+$), 283 ($M^+$+1), 284 ($M^+$+2). Anal. calcd. (%) for $C_{11}H_{10}N_2O_5S$ C, 46.81; H, 3.57; N, 9.92; S, 11.36. Found: C, 46.32; H, 3.46; N, 9.94; S, 11.42.

*2.2.2.2. 4-Hydroxy-3-[(1E)-1-({[(1E)-1-(4-hydroxy-2-oxo-2H-chromen-3-yl)ethylidene]sulfamoyl}imino)ethyl]-2H-chromen-2-one (**2h**).* Two equivalents of sulfamide were added to a 50 mL methanol solution of 3-acetyl-4-hydroxychromene-2-one (**1**) (0.5 g, 2.45 mmol). The mixture was heated under microwaves for 10 min. After cooling, the solvent was removed and the obtained solid filtered and re-crystallized from methanol. Yellow crystals, yield: 44%, mp: 276–277 °C. IR (KBr): $\upsilon_{max}$ $cm^{-1}$ 3428, 3052, 3016, 2929, 2848, 1694, 1678, 1613, 1574, 1482, 1459, 1382, 1146. $^1H$ NMR (200 MHz, DMSO-$d_6$): $\delta$ ppm 14.48 (br s, 1H, OH), 7.73–6.96 (m, 4H, C—H-5, C—H-6, C—H-7, C—H-8), 2.97 (s, 3H, $CH_3$—C). $^{13}C$ NMR (50 MHz, DMSO): $\delta$ ppm 175.90, 173.42, 161.64, 153.37, 132.23, 124.69, 123.84, 115.77, 116.46, 100.65, 17.86. MS: *m*/*z* 452 ($M^+$), 453 ($M^+$+1), 454 ($M^+$+2). Anal. calcd. (%) for $C_{23}H_{20}N_2O_6S$: C, 61.05; H, 4.46; N, 6.19; S, 7.05. Found: C, 61.32; H, 4.39; N, 6.17; S, 6.99.

### 2.3. Procedures for in vivo experiments

#### 2.3.1. Animal treatment

Experiments were performed on 2.5-month-old adult albino Wistar rats, weighing 220–250 g, kept at 12 h dark/light intervals, 22±2°C, and 50% relative humidity. The animals were fed with commercial rat food that was available *ad libitum*. All the animal procedures were approved by the Committee for Ethical Animal Care and Use of the Institute for Biological Research, Belgrade, which acts in accordance with the Guide for the Care and Use of Laboratory Animals, published by the US National Institute of Health (NIH Publication No. 85/23, revised in 1986). Compounds were dissolved in 0.9% NaCl solution, and three different concentrations, 0.5, 1, and 2 mg/kg of body weight (Kataranovski et al., 2007), were applied to obtain the proper dose–response. The positive control was warfarin solution, while the negative one was 0.9% NaCl. Each concentration of a single compound and each control were applied *intraperitoneally* (*i.p.*) to five animals. Animals were treated for seven days and received one dose of compounds per day. On the eighth day the animals were sacrificed and plasma, serum, and liver samples were collected.

### 2.3.2. Determination of prothrombin time

The plasma for determination of prothrombin time was prepared by the Quick method (Quick et al., 1935), immediately immersed in liquid nitrogen, and stored until usage at -80C. Coagulation experiments were performed on a MYTHIC 22-Orphee hematology analyzer. Prothrombin time (PT) was measured by Quick method (Quick et al., 1935) and results are presented in seconds (Table 1). For the purpose of 3-D pharmacophore generation, the results of anticoagulant activity determinations were converted into $EC_{200}$ values, i.e., the concentrations that will increase prothrombin time values by 200%. They were calculated from the dose–response curve (Bhatia et al., 2009) by taking the highest activity value of the most active compound as 100% of activity, after the results having been expressed as kg/kg values. The $EC_{200}$ values were calculated with OriginPro 8 statistical software (OriginLab Corporation, Northampton, MA, USA, 2009) using the Linear Dose–response function for compounds **2a** and **2f** (Fig. 1) and the Nonlinear Curve Fit Growth/Sigmoidal Dose–response function for the remaining derivatives (Fig. 1 and Table 1). The $EC_{200}$ values were then converted into $pEC_{200}$ by taking Log (1/$EC_{200}$).

### 2.3.3. Measurement of serum biochemical markers

The serum for determination of biochemical parameters, aspartate transaminase (AST), alanine transaminase (ALT), alkaline phosphatase (ALP), and bilirubin was prepared by the Quick method (Quick et al., 1935), immediately immersed in liquid nitrogen, and stored until usage at -80C. The catalytic activities of AST and ALT at 340 nm, and ALP at 405 nm, were determined by UV–Vis kinetic methods according to the recommendations of the Expert Panel of the IFCC (International Federation of Clinical Chemistry)

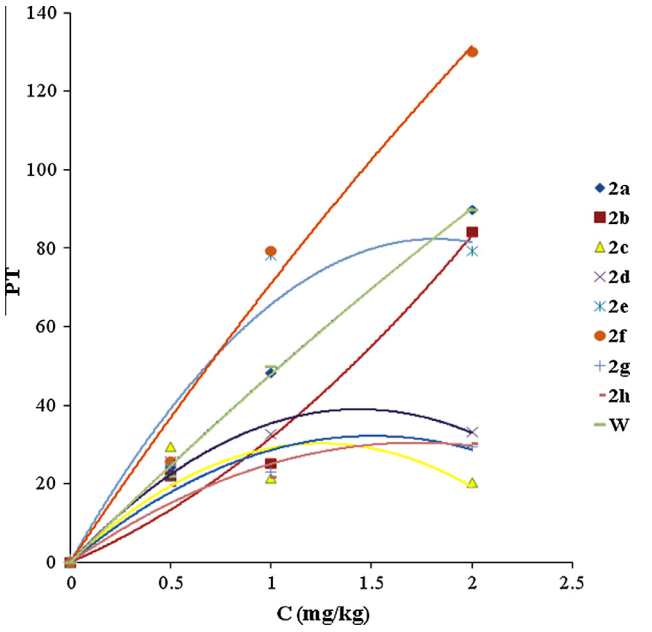


**Fig. 1.** Dose–response curve of *in vivo* anticoagulant activity of compounds **2a**–**2h.**

**Table 1**
Coagulation parameters and values of serum biochemical markers after seven days of *intraperitoneal* application of compounds **2a**–**h** to adult male Wistar rats.

| Comp. | Conc. (mg/kg) | PT (s) | AST (U/l) | ALT (U/l) | ALP (U/l) | Bilirubin (μmol/l) |
|---|---|---|---|---|---|---|
| **2a** | 0.5 | [a]24.2 ± 0.5*† | 81.89 ± 0.24*† | 31.86 ± 0.14* | 383.10 ± 0.25*† | 28.42 ± 0.25*† |
| | 1 | 48.4 ± 0.5*‡ | 103.89 ± 0.28*‡ | 39.29 ± 0.23*‡ | 355.41 ± 0.14*‡ | 44.08 ± 0.32*‡ |
| | 2 | 90.0 ± 0.9* | 58.58 ± 0.32*§ | 26.63 ± 0.24*§ | 412.82 ± 0.38*§ | 30.49 ± 0.17* |
| **2b** | 0.5 | 22.0 ± 0.2* | 52.60 ± 0.46*† | 43.65 ± 0.22*† | 348.45 ± 0.45*† | 44.11 ± 0.35*† |
| | 1 | 25.3 ± 0.7*‡ | 73.50 ± 0.25*‡ | 46.71 ± 0.41*‡ | 345.05 ± 0.35*‡ | 26.51 ± 0.41*‡ |
| | 2 | 84.3 ± 0.9*§ | 52.47 ± 0.18*§ | 29.25 ± 0.15*§ | 353.27 ± 0.26*§ | 33.07 ± 0.36*§ |
| **2c** | 0.5 | 29.5 ± 0.3*† | 59.89 ± 0.47*† | 27.06 ± 0.26*† | 289.85 ± 0.42*† | 39.80 ± 0.32*† |
| | 1 | 21.5 ± 0.4*‡ | 79.18 ± 0.25*‡ | 30.99 ± 0.24*‡ | 323.56 ± 0.13*‡ | 25.85 ± 0.41* |
| | 2 | 20.5 ± 0.4*§ | 123.09 ± 0.23*§ | 29.25 ± 0.17*§ | 551.59 ± 0.18*§ | 32.31 ± 0.35*§ |
| **2d** | 0.5 | 25.8 ± 0.4*† | 85.55 ± 0.24*† | 44.96 ± 0.19*† | 446.54 ± 0.46*† | 27.93 ± 0.21*† |
| | 1 | 32.8 ± 0.6*‡ | 78.57 ± 0.15* | 34.48 ± 0.16*‡ | 439.74 ± 0.24*‡ | 39.67 ± 0.41*‡ |
| | 2 | 33.4 ± 0.8*§ | 80.32 ± 0.16*§ | 30.99 ± 0.35*§ | 389.13 ± 0.32*§ | 35.89 ± 0.32*§ |
| **2e** | 0.5 | 22.1 ± 0.3* | 105.20 ± 0.24*† | 43.65 ± 0.42*† | 456.13 ± 0.21*† | 32.10 ± 0.41*† |
| | 1 | 78.4 ± 0.6*‡ | 115.24 ± 0.21*‡ | 41.90 ± 0.16*‡ | 545.47 ± 0.24*‡ | 29.13 ± 0.21*‡ |
| | 2 | 79.4 ± 0.6* | 139.24 ± 0.22*§ | 53.69 ± 0.27*§ | 414.26 ± 0.56*§ | 54.04 ± 0.41*§ |
| **2f** | 0.5 | 25.8 ± 0.5*† | 94.80 ± 0.15*† | 47.58 ± 0.34*† | 388.28 ± 0.52*† | 41.47 ± 0.25*† |
| | 1 | 79.3 ± 0.6*‡ | 107.51 ± 0.24*‡ | 54.56 ± 0.24*‡ | 520.68 ± 0.61*‡ | 33.43 ± 0.21*‡ |
| | 2 | 130.0 ± 1.1*§ | 108.41 ± 0.14*§ | 48.89 ± 0.35*§ | 415.20 ± 0.34*§ | 37.96 ± 0.21*§ |
| **2g** | 0.5 | 25.1 ± 0.2*† | 90.42 ± 0.23*† | 40.81 ± 0.41*† | 445.69 ± 0.33*† | 21.46 ± 0.16*† |
| | 1 | 23.1 ± 0.2*‡ | 98.28 ± 0.14*‡ | 37.32 ± 0.35*‡ | 572.65 ± 0.18*‡ | 27.09 ± 0.21*‡ |
| | 2 | 29.6 ± 0.2*§ | 98.21 ± 0.27*§ | 26.98 ± 0.51*§ | 374.43 ± 0.25*§ | 16.17 ± 0.41*§ |
| **2h** | 0.5 | 19.55 ± 0.3*† | 92.69 ± 0.52† | 48.02 ± 0.15*† | 370.70 ± 0.47*† | 29.22 ± 0.35*† |
| | 1 | 21.7 ± 0.4*‡ | 93.85 ± 0.43*‡ | 35.79 ± 0.26*‡ | 341.48 ± 0.26*‡ | 28.42 ± 0.36*‡ |
| | 2 | 30.25 ± 0.4*§ | 106.51 ± 0.35*§ | 43.87 ± 0.27*§ | 474.65 ± 0.51*§ | 43.06 ± 0.25*§ |
| **W** | 0.5 | 21.95 ± 0.2* | 92.10 ± 0.24 | 31.65 ± 0.41* | 479.15 ± 0.21* | 46.97 ± 0.52* |
| | 1 | 49.8 ± 0.6* | 97.48 ± 0.22* | 31.43 ± 0.31* | 313.97 ± 0.33* | 25.35 ± 0.23* |
| | 2 | 89.8 ± 0.4*§ | 106.07 ± 0.32*§ | 39.29 ± 0.47*§ | 417.49 ± 0.14*§ | 30.30 ± 0.45*§ |
| **C** | | 14.5 ± 0.1 | 92.80 ± 0.21 | 29.25 ± 0.42 | 376.18 ± 0.35 | 15.73 ± 0.36 |

[a] Values are presented as means ± SD (standard deviation) obtained from 3 independent experiments; $n = 50$ rats; 5 rats/group.
* $p < 0.05$ When compared with negative control group.
† $p < 0.05$ When compared with warfarin in concentration of 0.5 mg/kg.
‡ $p < 0.05$ When compared with warfarin in concentration of 1 mg/kg.
§ $p < 0.05$ When compared with warfarin in concentration of 2 mg/kg.

(Bergmeyer et al., 1976; Bergmeyer and Hørder, 1980; Walters and Gerarde, 1970). Colorimetric methods were used to determine total bilirubin on 550 nm (Jendrassik and Gróf, 1938). All kinetic and colorimetric measurements were recorded using a Perkin–Elmer Lambda 25 UV/Vis spectrophotometer.

*2.3.4. Determination of antioxidant markers in liver homogenate*

Rat liver samples were homogenized in phosphate buffer (5 mM, pH = 7.4) to give a 10% (w/v) liver homogenate and then centrifuged at 4000 rpm for 15 min at 4 °C. The supernatant of liver homogenate was used for estimation of reduced glutathione (GSH) (Ellman, 1959) and catalase (CAT) (Góth, 1991) levels by the colorimetric method. The content of malonyldialdehyde (MDA) (Ohkawa et al., 1979) in the liver homogenate supernatant was determined using the standard compound 1,1,3,3-tetraethoxypropane. Total proteins concentration was determined according to the method of Lowry using the bovine serum albumin as the standard (Lowry et al., 1951). All colorimetric measurements were performed using a Perkin–Elmer Lambda 25 UV/Vis spectrophotometer.

*2.3.5. Histopathological studies*

Liver slices were fixed with 10% formalin in phosphate buffered saline for 24 h and embedded in paraffin. The 5 μm thick sections were made using a microtome, stained with haematoxylin–eosin, and observed under a microscope to determine histopathological changes in the liver (Mihailović et al., 2013). Photographs of each slide were taken at 100× magnification.

*2.3.6. Statistical evaluations*

Statistical evaluation of the data was performed by 1-way ANOVA analysis. Variance homogeneity and data distribution were determined with the Levene and Kolmogorov–Smirnov tests, respectively. Post-hoc comparison between the control and treated groups was performed with the T3 Dunnett's test or with the Bonferroni test when the variance was not homogeneous. Statistical analysis was performed using the SPSS statistical software package, version 13.0 for Windows (Coakes et al., 2006). The results were considered to be statistically significant at $p < 0.05$.

*2.4. Molecular modeling studies*

*2.4.1. Molecular optimization of tested compounds*

Molecular optimizations were performed to predict the bioactive conformations of tested compounds **2a**–**h**. The initial structures were built in Spartan 2008 (Wavefunction Inc., Irvine, USA, 2006) and imported into MacroModel 9.5 (Mohamadi et al., 1990) *via* graphical interface Maestro 9.0. Conformations were obtained by using the simulated annealing molecular dynamics procedure implemented in MacroModel as follows (Ragno et al., 2008). Each structure was energy minimized to a low gradient. The non-bonded cutoff distances for van der Waals interactions were set to 8 Å, while distances for electrostatic ones were set to 20 Å. An initial random velocity was applied to all atoms corresponding to 310 K. Three subsequent molecular dynamics simulations were then performed. The first was carried out for 10 ps with a 1.5 fs time-step at a constant temperature of 310 K for equilibration purposes. The next molecular dynamics simulation was carried out for 20 ps, during which the system was coupled to a 150 K thermal bath with the time constant of 5 ps. The time constant represents approximately the half-life for equilibration with the bath; consequently the second molecular dynamics command caused the molecule to slowly cool to approximately 150 K. The third and last dynamics simulation cooled the molecule to 50 K over 20 ps. A final energy minimization was then carried out for 250 iterations using a conjugate gradient. The minimizations and molecular dynamics were in all cases performed by implicit solvation in a simulated aqueous solution using GB/SA (Generalized Born solvent accessible surface area) keyword and the OPLS2005 force field. All ligands were furthermore individually inspected and the correct protonation states at pH 7.4 were considered and adjusted according to results obtained with the Protonation Major Microspecies tool of the MarvinSketch program (ChemAxon, Budapest, Hungary, 2012).

*2.4.2. Molecular docking studies and energy minimization of ligand–enzyme complexes*

The complete crystallized three-dimensional structure of transmembrane rat VKORC1 is currently not available from the Brookhaven Protein Data Bank. The structure of homology-modeled rat VKORC1 built in our laboratory was therefore used as a molecular target in docking experiments. The homology modeling protocol in the complete membrane-aqueous system consisted of the 1,2-dimiristoyl-SN-3-phosphorylcholine (DMPC) model, was described in detail in our previous paper (Mladenović et al., 2012). The protein structure was prepared for molecular docking in the following way. Hydrogen atoms were added using the leap module of the Amber suite (Case et al., 2006) implemented in the UCSF Chimera program (Pettersen et al., 2004). All amino acids in the protein were additionally inspected individually and correct protonation states at pH = 7.4 were considered, i.e., lysines, arginines, aspartates and glutamates were assumed to be in the ionized form, and parameters were calculated using the Antechamber module of the Amber suite.

The protein structure was further incorporated into the AutoDockTools graphical user interface. Nonpolar hydrogen atoms were removed, while Gasteiger charges and solvent parameters were added. All of the tested compounds were used as ligands for docking. The rigid root and rotable bonds were defined using AutoDockTools. The docking was performed with AutoDock 4.2 (Morris et al., 1996). Dimensions of the grids were 16 Å × 22 Å × 30 Å, with a spacing of 0.375 Å between the grid points and center grid box coordinates $x = 31.456$, $y = 65.386$, and $z = 13.274$, referring to the enzyme active site: Thr138, Tyr139, and Ala140. The Lamarckian Genetic Algorithm was used to generate orientations or conformations of ligands within the binding site. The global optimization started with a population of 200 randomly positioned individuals, a maximum of $1.0 \times 10^6$ energy evaluations, and a maximum of 27.000 generations. A total of 100 runs were performed with RMS Cluster Tolerance of 0.5 Å.

Finally, a molecular mechanics approach was applied to refine the Autodock output. The computational protocol included the application of 10.000 steps of the steepest descent algorithm until the derivative convergence was 0.01 kcal/Å mol. An AMBER force field with the continuum GB/SA salvation model (water as solvent) implemented in MacroModel was used during minimization. Moreover, because of the large number of atoms in the model, some additional constraints had to be imposed to correctly optimize the complexes obtained by the docking. A subset, comprising only inhibitors and shells of residues possessing at least one atom at a distance of 5 Å from any of the inhibitor atoms, was created and subjected to energy minimization. The inhibitors and all the amino acid side chains of the shell were unconstrained during energy minimization to allow for reorientation and proper hydrogen-bonding geometries and van der Waals contacts. All the atoms not included in the above-defined subset were fixed, but their non-bond interactions with all of the relaxing atoms have been calculated.

*2.4.3. Alignment of **2a**–**h** bioactive conformations*

In order to reduce any geometric inaccuracy of the obtained ligand–VKORC1 complexes, all complexes were superimposed using

the **2f**–VKORC1 complex as a template. This complex was chosen to be the template because compound **2f** was the most active one. Superimposition of the obtained complexes was carried out with the aid of the UCSF Chimera program using the command-line implementation of MatchMaker. By applying this protocol, all ligands were not actually atom-by-atom aligned, but were rather placed in the equivalent positions with respect to their interaction within the receptor. In this sense, much better representation of alignment of the bioactive conformations was achieved.

*2.4.4. Receptor-based pharmacophore model generation*

The structures of **2a**–**2h** in complex with VKORC1 (Fig. S2, Supplementary information) were used as starting structures for the generation of pharmacophore models in the present study. The LigandScout 2.0 software was applied for the detection and interpretation of crucial interaction patterns between VKORC1 and the ligand. LigandScout (Wolber and Langer, 2005) extracts and interprets the ligand and the macromolecular environment from the PDB file, then automatically creates and visualizes an advanced pharmacophore model. The pharmacophore was exported as a hypoedit script and converted into Discovery Studio 2.5 (Accelrys Software Inc., San Diego, USA, 2012) format with the Hypoedit tool. The bound ligand was converted to shape query and merged with the pharmacophore model to give a combined feature-shape query, which was used for *in silico* screening.

All the pharmacophore modeling calculations were carried out using the Catalyst 4.11 software package (Accelrys Software Inc., San Diego, USA, 2012). The common pharmacophore features necessary for potent VKORC1 inhibitors were identified with the aid of HipHop program, while quantitative pharmacophore models were created by the *HypoGen* module within Catalyst. The common feature hypotheses, i.e., qualitative models, were produced by comparing the set of conformational models with a number of 3-D configurations of chemical features shared among the training set molecules. This analysis results in a qualitative model wherein important chemical features can be easily identified. Activity of the training set was predicted by creating a 3-D pharmacophore, which was used for quantitative assessment of the best qualitative model. The quality of models is best described in terms of fixed cost, null cost, total cost, root mean square deviation, and other statistical parameters.

*2.4.5. External validation of the pharmacophore model using the test set method*

External validation of the obtained 3-D pharmacophore model was performed using a test set that consisted of 16 4-hydroxycoumarins, namely **ts-1-10c** (Fig. S5, Supplementary information), which were previously announced as *in vivo* anticoagulants (Mladenović et al., 2012). The test set compounds contain various C-3 substituents like carbonyl and carboxyl groups linked to coumarin core *via* a 3-methylbut-2-en-yl scaffold on one side and thiazole-*N*-phenyl residues on the other. Their anticoagulant activity *in vivo* was obtained previously in similar experimental conditions (Mladenović et al., 2012), and $pEC_{200}$ values were calculated for the purpose of this study. The test set molecules were optimized in MacroModel and docked into the active site of rat VKORC1 by Autodock 4.2 using the same setup as described here. By means of this procedure, docking assessment was performed (Fig. S6, Supplementary information) to align the test set compounds into the VKORC1 active site. External validation on structurally very different compounds confirmed the quality of the training set 3-D pharmacophore model.

The generated hypothesis was validated mainly to check whether the best hypothesis selected active compounds of the test set during the screening process by means of determining the correlation between experimental and predicted activity.

*2.4.6. ADMET prediction*

ADMET descriptors allow us to eliminate compounds with unfavorable ADMET characteristics so as to avoid expensive reformulation later. They also enable us to evaluate proposed structural refinements designed to improve ADMET properties prior to resource expenditure on synthesis (Zhang et al., 2012). The pharmacokinetic profile of tested compounds was predicted by the ADMET descriptors protocol in Discovery Studio 2.5. The ADMET descriptors were intestinal absorption, aqueous solubility, blood–brain barrier (BBB) penetration, Cytochrome P450 2D6 enzyme inhibition, hepatotoxicity, plasma-protein binding (PPB), atom-based Log*P* (Alog*P*), and polar surface area (PSA).

## 3. Results and discussion

### 3.1. Synthesis

Two synthetic procedures, conventional and microwave-assisted, were used for preparation of the examined compounds. Different synthetic procedures resulted in different types of products.

Using the conventional procedure, 3-(1-aminoethylidene)chroman-2,4-diones, **2a**–**f**, were synthesized in the presence of $Et_3N$ by the condensation of starting compound 3-acetyl-4-hydroxycoumarin (**1**) with the corresponding primary amine (Scheme 1). The condensation reaction induced intramolecular tautomerization of the 4-hydroxyl group of the coumarin core. Thus, instead of an imino group, a secondary amino group was formed, along with an external double carbon bond. The reaction between equimolar amounts of all reagents yielded compounds **2a**–**d** which contain one chroman-2,4-quinone ring. On the other hand, two equivalents of $Et_3N$ gave **2e** and **2f**, compounds with two chroman-2,4-quinone cores in the structure. Accordingly, it must be acknowledged that the synthesis of **2b** is not new (Małecka et al., 2004; Budzisz et al., 2003). However, the applied experimental procedure significantly improved the yield of the product. Elemental analysis and spectral data (IR, $^1$H NMR, $^{13}$C NMR, GC/MS) of the synthesized compounds were in full agreement with the suggested molecular structures. The absence of a signal for the hydroxyl group at position C-4 in $^1$H NMR spectra, as well as the presence of low intensity bands at 3420–3412 cm$^{-1}$ in IR and broad singlets at 14.00–11.08 ppm in $^1$H NMR spectra that correspond to an NH proton, confirmed the tautomerization of compounds **2a**–**f**. In addition to this conclusion, $^{13}$C NMR showed signals corresponding to two different carbonyl groups and carbons which form an external double bond.

On the other hand, the reaction under microwave irradiation in the absence of $Et_3N$ and presence of sulfamide as a reagent led to the formation of 4-hydroxycoumarin Schiff base adducts **2g** and **2h** (Scheme 1), without intramolecular tautomerization. Using equimolar amounts of reagents, monosubstituted sulfamide derivative **2g** was formed, while the presence of two equivalents of sulfamide yielded disubstituted **2h**. $^1$H NMR showed broad singlets at 13.86 and 14.48 ppm, assigned to 4-OH of **2g** and **2h**, respectively. The formation of an imino group was confirmed by a strong C=N band in the IR spectra at 1678–1674 cm$^{-1}$.

The main advance of the conventional synthetic approach is its high efficiency in terms of product yield and in particular one-step formation of compounds that are structurally similar to vitamin K-2,3-epoxide and are therefore recognized by the ligand-based approach as inhibitors of the coagulation cycle *in vivo*. On the other hand, by utilizing the microwave-assisted procedure, novel 4-hydroxycoumarins were synthesized, i.e., compounds were formed that can undergo the required tautomerization in an *in vivo* environment (Mladenović et al., 2012).

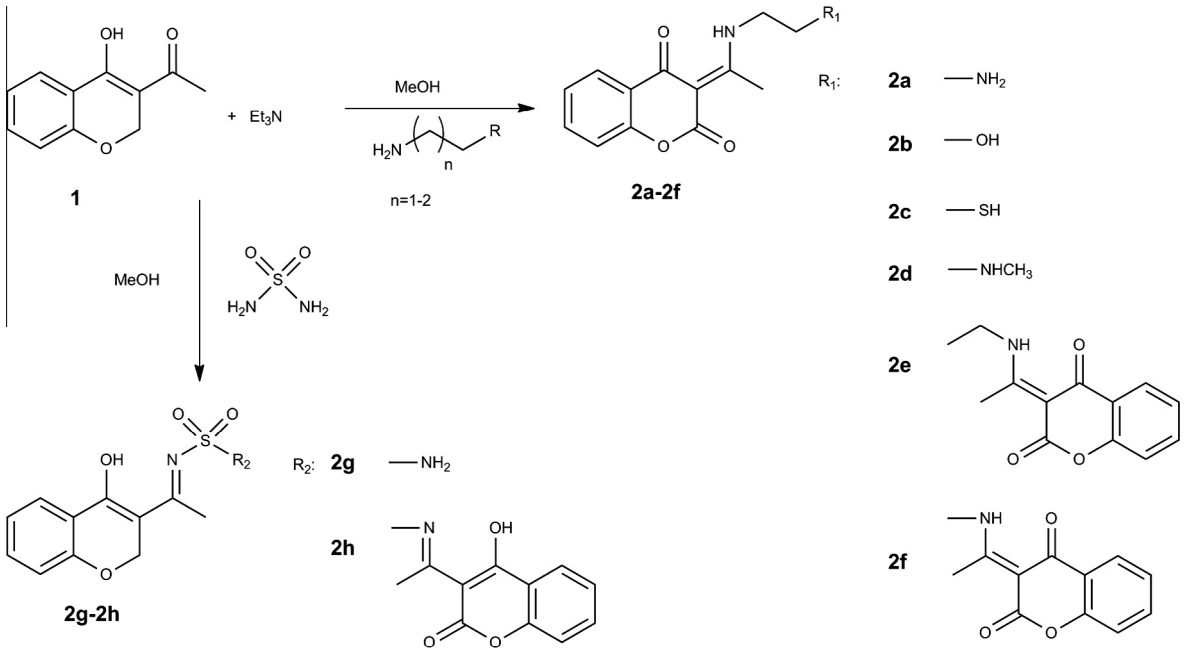


**Scheme 1.** General synthetic procedure for compounds **2a**–**f** and **2g**–**h**.

### 3.2. In vivo anticoagulant activity

Table 1 summarizes anticoagulant activity of the tested compounds applied *intraperitoneally* (*i.p.*) to adult Wistar rats in three different concentrations, viz., 0.5, 1, and 2 mg/kg of body weight. Three different doses were chosen since we wanted to obtain the correct dose response, calculate the concentration of compounds that increase prothrombin time by 200%, and avoid the death of experimental animals (as much as the $LD_{50}$ of our compounds is unknown). Moreover, seven-day continuous treatment was chosen because warfarin and other clinically used anticoagulants exhibit anticoagulant activity only upon long-term application (Jaffer and Bragg, 2003).

Although clinically used anticoagulants are applied orally, *i.p.* administration was chosen in the current stage of evaluation as a way of treatment in order to obtain the full effect of the tested compounds in the applied concentrations. The full effect is realized because anticoagulants inhibit the liver enzyme VKORC1, and *i.p.* applied compounds are transferred directly into the liver (Lukas et al., 1971). Owing to this, instant interaction between the compounds and VKORC1 was induced. Even though *i.p.* delivery is considered to be a parenteral route of administration, the primary route of absorption is into the mesenteric vessels that drain into the portal vein and pass through the liver (Lukas et al., 1971). Lukas and co-workers also demonstrated that compounds administered *i.p.* are absorbed primarily through the portal circulation and, therefore, must pass through the liver before reaching other organs. In our study, *i.p.* injection (an acceptable alternative method of introducing substances into an animal) was chosen instead of oral administration to ensure that each animal received an accurate dose, in a manner less likely to cause injury.

The activity of compounds was examined only *in vivo* since the pharmacology of inhibition of the coagulation cycle by coumarin and related anticoagulants is meaningful only when the activity is considered on the molecular level, i.e., if anticoagulants inhibit the vitamin K cycle. Compounds **2a**–**2f** are by structure competitive inhibitors of vitamin K-2,3-epoxide and therefore are recognized as VKORC1 inhibitors. On the other hand, compounds **2g**–**h** contain a 4-hydroxycoumarin ring, which also exists in the structure of warfarin. Thus, they represent potential anticoagulants. Insight into the structural features that determined activity of each compound was obtained upon examination of results relating to each applied concentration.

After the administration of compounds in a concentration of 0.5 mg/kg, the following decreasing order of activity was observed: **2c** > **2d** = **2f** > **2g** > **2a** > **2e** > **2b** > **W** > **C** > **2h**. As many as seven compounds presented better anticoagulant activity than warfarin. That was unsurprising since warfarin is known to exert good anticoagulant activity after continuous several-day application in higher concentrations (Jaffer and Bragg, 2003). In comparison with saline (0.90% w/v of NaCl, **C**) as the negative control (PT = 14.5 s) and warfarin, **W** (PT = 21.95 s) as the positive control, the range of activity of active compounds was PT = 22.0–29.5 s. Some information about structure–activity relationships was obtained. It was clear that the compounds containing a chroman-2,4-quinone core (**2a**–**f**) were generally better anticoagulants than 4-hydroxycoumarins (**2g**–**h**).

With increase of the dose, compounds containing ethane-1,2-diamine (**2f**, PT = 79.3 s) and propane-1,3-diamine (**2e**, PT = 78.4 s) residues as integral parts of C-3 scaffolds were better anticoagulants than warfarin (PT = 49.8 s). It should be noted that compounds **2e** and **2f** contain an additional chroman-2,4-dione ring as a substituent of the terminal amino group. The rest of the compounds did not present better anticoagulant activity in comparison with warfarin. The activity of **2a** (which contains an ethane-1,2-diamine scaffold) was slightly lower and comparable to that of warfarin.

In the highest concentration, only **2f** (PT = 130.0 s) and **2a** (PT = 90.0 s) showed better anticoagulant activity than that of wafarin. From the obtained results, it is clear that the presence of chroman-2,4-dione on the one hand, and ethylenediamine as an integral part of C-3 residues on the other is of crucial importance for high *in vivo* activity of the tested compounds.

The arbitrary decision to treat the animals with three different doses was validated by the obtained distinctly linear dose–response curve for the most active compounds, **2a** and **2f** (Fig. 1). The presented results are in accordance with the well-known anticoagulant behavior of warfarin, whose anticoagulant behavior is

linked with its ability to increase prothrombin time with an increase of the applied concentration (Jaffer and Bragg, 2003). Since only **2a** and **2f** showed a linear dose–response, as discerned by close inspection of Fig. 1, the other compounds cannot be classified as anticoagulants, inasmuch as their activity dropped with increase of concentration. We intend to investigate oral application of the most active compounds and evaluate their anticoagulant activity in future work.

### 3.3. Estimation of chemically induced hepatocyte damage after administration of the compounds

Chemically induced hepatic toxicity in rats was evaluated by determining the catalytic activities of serum AST, ALT, and ALP as hepatocellular markers, and by monitoring the bilirubin concentration as a hepatobiliary marker (Singh, 2000; Tennant, 1999; Marschall et al., 2005). The AST, ALT, and ALP catalytic activities are sensitive indicators of acute liver damage (Singh, 2000). Upon chemically induced damage to hepatocytes of the cell membrane, the catalytic activity of AST and ALT is increased and the enzymes are released into the extracellular environment (Nalpas et al., 1986). Since ALP is an extracellular enzyme, its catalytic activity is not so reliable as an indicator of necrosis (Kaplan and Righetti, 1970). Biochemical screening was performed on serum samples obtained after the application of compounds in all three concentrations (Table 1). Bilirubin concentration is a useful clinical parameter for the diagnosis of bile damage (Manokaran et al., 2008).

The catalytic activity of AST grew with increase in the applied concentration of **2f**, but it was quite comparable with the positive control. Thus, in serum containing **2f,** the catalytic activity of AST was increased in comparison with the negative control and warfarin: 1.02-, 1.16-, and 1.17-fold above values measured in the negative control; and 1.02-, 1,10-, and 1.02-fold above those in the positive one. This indicated that **2f** induced little or no inflammation of hepatocytes. In addition, the slight change in catalytic activity of ALP with an increase of concentration (1.03-, 1.52-, and 1.11-fold above the negative control value, respectively) suggested that **2f** induced inflammation but no severe necrosis of hepatocytes. On the other hand, **2a** behaved in an anti-inflammatory manner, since the catalytic activity of AST decreased with increase in concentration of the compound. Thus, in serum containing 2 mg/kg of **2a,** the catalytic activity of AST was even lower than in the negative control, 63.13% of the basic value. A similar pattern was observed for the catalytic activity of ALT. To judge from the concentration of total bilirubin, there was no damage to bile after the application of **2a** and **2f**. The maintained or even decreased catalytic activity of enzymes with increase of concentration may be associated with the fact that the compounds probably are easily excreted (Killard et al., 1996) in the form of 7-hydroxy-glucuronides, i.e., they are not accumulated in the rat body.

A second evaluation of toxicity of **2f** and **2a** was performed by determining the level of induced oxidative stress using the GSH, CAT, and MDA as antioxidant markers. These additional tests were performed because consumption of compounds that might generate free radicals can induce pathogenesis of a wide range of diseases: hypertension (Lassegue and Griendling, 2004), Alzheimer's and Parkinson's diseases (McIntosh et al., 1997), and cancer (Festa et al., 2001) after radical-induced DNA double-strain breaks. The concentrations of GSH and MDA and catalytic activity of CAT (Table 2) in liver homogenate were expressed as equivalents of total protein concentration (TP).

If the presence of a xenobiotic induces generation of oxidative species in the cell, the concentration of GSH decreases, since the thiol group of cysteine is able to donate a reducing equivalent to reduce the quantity of other unstable molecules (Scholz et al., 1989). Thus, with increase of **2f** concentration in liver homogenate, a minor decrease in GSH concentration was recorded: 1.40-, 1.24-, and 1.12-fold in relation to the basal value measured in the negative control. The results suggested that **2f** could be involved in the generation of oxidative stress. On the other hand, GSH concentration increased in samples containing **2a**: 1.34-, 1.32-, and 1.37-fold above the basal value in the negative control, suggesting that this compound is not an inducer of oxidative stress. The results obtained for **2f** raised the question of whether or not the examined compounds form a covalent bond with GSH. A coumarin or chromen ring itself not substituted at position C-3 can form a covalent bond with GSH *via* the thiol group (Zhuo et al., 2009). This metabolic pathway results in the formation of 3-glutathionyl-4-hydroxy-3,4-dihydroxycoumarin and 4-glutathionyl-4-hydroxy-3,4-dihydroxycoumarin, species that arise after the addition of a thiol group to coumarin-3,4-epoxide. That particular epoxide is singled out as the primary toxic reactive intermediate for liver microsomes, as inasmuch epoxidation of the coumarin core by CytP450 is the main bioactivation pathway. Analysis of the data presented in Table 2 reveals that with an increase in concentration of the compounds, there is a decrease in the level of GSH. This further implies that there is no production of the 3,4-epoxide as a reactive intermediate during the metabolic activation of our compounds. These results correlate with the *in vivo* toxicology findings, which suggest that there is no tissue-selective toxicity induced by activation of the target compounds. The above statement is further supported by the fact that there are no literature data describing the genesis of warfarin-3,4-epoxide in the metabolic activation of this clinical anticoagulant. It follows that coumarin or chromen-based compounds substituted in the C-3 position are most certainly not susceptible to condensation with GSH and do not represent potential toxicity on that level.

Additional information about whether or not **2f** and **2a** can produce reactive oxygen species was obtained with the remaining antioxidant markers. Loss of CAT activity is associated with increased susceptibility to oxidative stress (Milton, 2008). It follows that, CAT can be a sensitive indicator of oxidative cell damage. In liver homogenate samples containing **2f** and **2a,** catalytic activity of CAT rose progressively with increase in concentration of the compounds concentration: 2.45-, 2.50-, and 2.67-fold above the basic value measured in the negative control in samples of **2f**; and 1.62-, 2.04-, and 2.19-fold above that value in samples of **2a**. This was strong evidence indicating that the most active compounds are not oxidative stress inducers.

Final evaluation was obtained by measuring the concentration of malonyaldehyde (MDA). MDA is a product of increasing lipid peroxidation, which occurs after oxidative damage to lipoproteins in the cell membrane (Aitken et al., 1993). Increase of MDA concentration therefore suggests severe damage to the cell membrane. MDA concentration decreased in samples of **2f** and remained similar in samples of **2a** in comparison with the negative control, providing final proof that the most active compounds are non-toxic and incapable of causing oxidative stress.

### 3.4. Histopathological studies

To complete the estimation of chemically induced liver damage, thorough histopathological examination was performed on liver samples taken from animals that were treated with **2f**, **2a**, and **W** in the highest dose of 2 mg/kg. Only the highest concentration was taken into account since it led to the best dose–response for **2a** and **2f**. The results of histopathological analyses are summarized in Table 3 and Fig. 2. In comparison with the negative control (Table 3 and Fig. 2d), where only passive hyperemia (congestion) was perceived, warfarin (Fig. 2c) induced severe liver damage reflected by moderate enlargement of portal spaces and followed by infiltration of lymphocytes, leukocytes, and macrophages

**Table 2**
Total protein content and catalytic activity of liver antioxidant enzymes after seven days of *intraperitoneal* application of compounds **2a**–**h** to adult male Wistar rats.

| Comp. | Conc. (mg/kg) | TP (g/l) | GSH (mg/g) | CAT (μmol/mg) | MDA (nmol/mg) |
|---|---|---|---|---|---|
| **2a** | 0.5 | 26.86 ± 0.14[a] | 9.44 ± 0.22*† | 11.27 ± 0.24*† | 0.47 ± 0.06† |
| | 1 | 26.02 ± 0.12 | 9.19 ± 0.14*‡ | 14.23 ± 0.12*‡ | 0.47 ± 0.03*‡ |
| | 2 | 25.52 ± 0.23 | 9.54 ± 0.21* § | 15.30 ± 0.15* § | 0.48 ± 0.01* § |
| **2b** | 0.5 | 23.56 ± 0.16 | 8.18 ± 0.23*† | 18.22 ± 0.13*† | 0.60 ± 0.02*† |
| | 1 | 20.86 ± 0.32 | 10.02 ± 0.21*‡ | 20.59 ± 0.24*‡ | 0.56 ± 0.12*‡ |
| | 2 | 26.61 ± 0.17 | 7.68 ± 0.17*§ | 23.52 ± 0.13*§ | 0.52 ± 0.06*§ |
| **2c** | 0.5 | 29.53 ± 0.28 | 9.30 ± 0.36* † | 9.35 ± 0.17* | 0.63 ± 0.03* † |
| | 1 | 25.67 ± 0.16 | 9.08 ± 0.14*‡ | 15.48 ± 0.62*‡ | 0.63 ± 0.01* |
| | 2 | 27.29 ± 0.14 | 10.22 ± 0.16*§ | 12.35 ± 0.32*§ | 0.78 ± 0.08*§ |
| **2d** | 0.5 | 15.22 ± 0.32 | 12.36 ± 0.51*† | 30.16 ± 0.45*† | 1.09 ± 0.10*† |
| | 1 | 16.09 ± 0.14 | 10.99 ± 0.41*‡ | 26.96 ± 0.24*‡ | 1.09 ± 0.15*‡ |
| | 2 | 14.67 ± 0.45 | 11.93 ± 0.31*§ | 29.29 ± 0.37*§ | 1.31 ± 0.24*§ |
| **2e** | 0.5 | 29.24 ± 0.16 | 6.29 ± 0.23*† | 13.02 ± 0.31*† | 0.41 ± 0.02† |
| | 1 | 20.60 ± 0.13 | 8.86 ± 0.13*‡ | 18.43 ± 0.25*‡ | 0.40 ± 0.02*‡ |
| | 2 | 15.99 ± 0.27 | 12.94 ± 0.16*§ | 23.24 ± 0.31*§ | 0.82 ± 0.26*§ |
| **2f** | 0.5 | 22.12 ± 0.24 | 9.52 ± 0.14*† | 17.08 ± 0.36*† | 0.52 ± 0.25*† |
| | 1 | 21.18 ± 0.23 | 8.68 ± 0.32*‡ | 17.44 ± 0.25*‡ | 0.52 ± 0.32*‡ |
| | 2 | 23.29 ± 0.14 | 7.84 ± 0.15*§ | 18.69 ± 0.26*§ | 0.42 ± 0.12*§ |
| **2g** | 0.5 | 20.61 ± 0.13 | 11.98 ± 0.61*† | 16.08 ± 0.31*† | 0.85 ± 0.15* |
| | 1 | 24.33 ± 0.17 | 10.50 ± 0.31*‡ | 13.68 ± 0.22*‡ | 0.87 ± 0.09*‡ |
| | 2 | 25.18 ± 0.23 | 9.34 ± 0.38*§ | 13.06 ± 0.28*§ | 0.70 ± 0.07*§ |
| **2h** | 0.5 | 21.78 ± 0.15 | 10.36 ± 0.42*† | 15.54 ± 0.31*† | 0.83 ± 0.06* |
| | 1 | 26.70 ± 0.16 | 10.83 ± 0.21*‡ | 8.74 ± 0.36*‡ | 0.84 ± 0.03*‡ |
| | 2 | 28.81 ± 0.18 | 8.76 ± 0.24*§ | 10.76 ± 0.25*§ | 0.64 ± 0.04* |
| **W** | 0.5 | 25.44 ± 0.34 | 10.28 ± 0.35* | 9.40 ± 0.26* | 0.84 ± 0.01* |
| | 1 | 21.34 ± 0.41 | 11.85 ± 0.23* | 16.49 ± 0.34* | 0.62 ± 0.05* |
| | 2 | 29.06 ± 0.34 | 9.92 ± 0.42* | 7.56 ± 0.15* | 0.64 ± 0.05* |
| **C** | | 30.75 ± 0.14 | 6.97 ± 0.21 | 12.23 ± 0.36 | 0.45 ± 0.03 |

[a] Values are presented as means ± SD obtained from 3 independent experiments; $n = 50$ rats; 5 rats/group.
* $p < 0.05$ When compared with negative control group.
† $p < 0.05$ When compared with warfarin in concentration of 0.5 mg/kg.
‡ $p < 0.05$ When compared with warfarin in concentration of 1 mg/kg.
§ $p < 0.05$ When compared with warfarin in concentration of 2 mg/kg.

**Table 3**
Morphological parameters of the rat liver upon seven-day continuous *i.p.* application of compounds **2a**–**2h**, warfarin, and the negative control in a concentration of 2 mg/kg of body weight.

| Comp. | Morphological parameters | | | | | | | | |
|---|---|---|---|---|---|---|---|---|---|
| | C[a] | DHL[b] | BD[c] | SR[d] | I[e] | FN[f] | PN[g] | BDR[h] | F[i] |
| **2a** | +[j] | | | | + | + | | | |
| **2b** | + | + | | | ++ | | | | |
| **2c** | + | | + | | + | + | | | + |
| **2d** | ++ | | | | ++ | + | | | |
| **2e** | + | | | | ++ | + | | | + |
| **2f** | + | | | | + | | | | |
| **2g** | + | | | | ++ | ++ | | | |
| **2h** | + | | | + | ++ | | | | |
| **W** | + | | | | + | ++ | ++ | + | |
| **C** | + | | | | | | | | |

[a] Congestion (passive hyperemia).
[b] Discontinued hepatocyte lines.
[c] Ballooning degradation.
[d] Signs of regeneration (rosettes, hypertrophy of nucleus).
[e] Infiltrations of lymphocytes, leukocytes and macrophages.
[f] Focal necrosis.
[g] Piecemal necrosis.
[h] Biliary ductular reaction.
[i] Fibrosis.
[j] +: minimal damage; ++: moderate damage; +++: massive damage; blank columns are referred to no visual damage.

(Table 3). Moreover, areas with moderate focal necrosis as well as ones with moderate piecemeal necrosis were spotted. In comparison with warfarin, **2f** (Fig. 2a) induced minor liver damage in the guise of infiltration of lymphocytes, leukocytes, and macrophages. The liver change noticed after application of **2a** (Fig. 2b) is characterized by minimal focal necrosis. The rest of the compounds (Table 3 and Fig. S1, Supplementary information) induced more liver damage. The general conclusion is that the most active compounds (**2a** and **2f**) do not induce any significant hepatocyte damage, as indicated by the observation of minor pathomorphological changes.

Photomicrographs of liver sections treated with the examined compounds and controls are presented in Fig. 2.

### 3.5. Insight into structural aspects required for anticoagulant activity

There is a great deal of controversy about the mechanism governing inhibition of the coagulation cycle by warfarin and related compounds. As warfarin inhibits the reduction of vitamin K-2,3-epoxide to vitamin K, where VKORC1 is converted from the reduced (active site sulfhydryl) to the oxidized (active site disulfide) form, it is a question of whether or not warfarin is covalently bound to the enzyme. The oxidized form is further reduced by DTT (Tie and Stafford, 2007) under *in vitro* conditions, while in the living cell the reduction is performed by microsomal NADH-dependent lipoamide reductase (Thijssen et al., 1994). But in view of the warfarin-mediated inhibition, preincubation of VKORC1 with DTT prior to warfarin incubation appears to diminish the inhibition of VKORC1 activity (Fasco et al., 1983). Experimental data suggest that warfarin rather binds to the oxidized form (Fasco et al., 1983) of VKORC1 than to the reduced one (Silverman, 1980). The inactivation of VKORC1 by warfarin occurs more rapidly when the enzyme is exposed to warfarin prior to DTT (Fasco et al.,

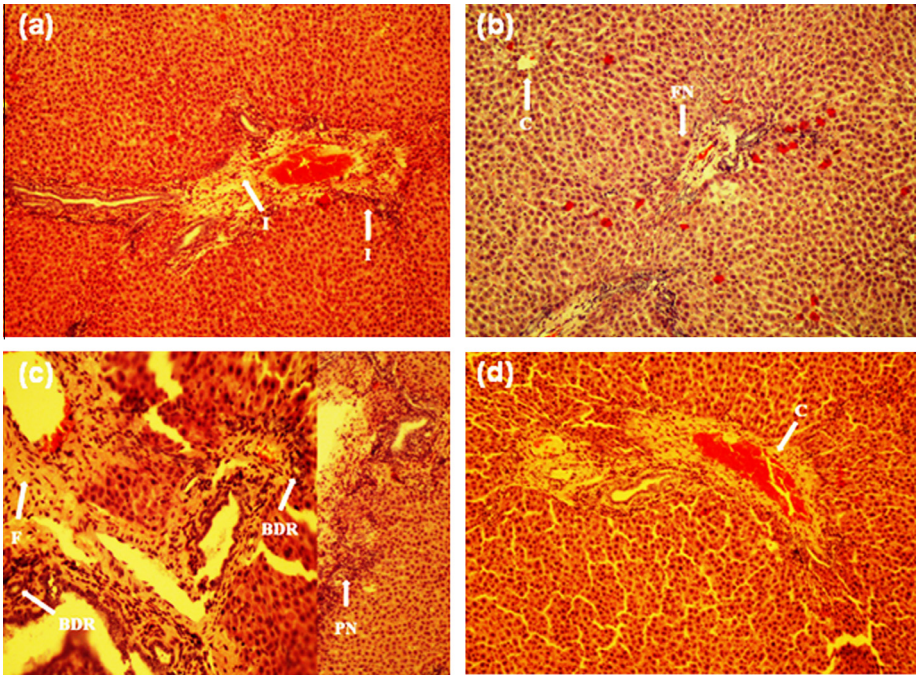


**Fig. 2.** Photomicrographs of liver sections treated with **2f** (a), **2a** (b), **W** (c), and **C** (d). Arrows: C – congestion; DHL – discontinued hepatocyte lines; BD – balloning degradation; SR – signs of regeneration (rosettes, hyperthrophy of nucleus); I – infiltrations of lymphocytes, leukocytes, and macrophages; FN – focal necrosis; PN – piecemal necrosis; BDR – biliary ductular reaction; F – fibrosis.

1983). Reduced lipoamide reductase stimulates VKORC1 activity *in vivo* with kinetics comparable with those of DTT, and is warfarin sensitive (Thijssen et al., 1994). Apart from the fact that the binding of vitamin K-2,3-epoxide or warfarin occurs on the oxidized form of VKORC1, the enzyme must be reduced in order to be activated prior to reaction with the epoxide or anticoagulant (Silverman, 1981). Only upon this activation is there an inhibition of the coagulation cycle by warfarin and related compounds.

Present knowledge indicates that warfarin cannot form an epoxide akin to vitamin K. Hence there is no possibility that the inhibition is performed by a covalent mechanism analogous to the one proposed for vitamin K 2,3-epoxide reduction (Tie and Stafford, 2007; Oldenburg et al., 2008). Since warfarin binding to VKORC1 is very tight, it was considered to be an irreversible process (Fasco and Principe, 1982). In support of irreversible inhibition, Silverman et al. proposed that the deprotonated form of warfarin is directly bound to reduced VKORC1 (Silverman, 1980). Contrary to Silverman's conclusion, it was recently confirmed that the oxidized form of VKORC1 represents the target for warfarin (Gebauer, 2007; Bevans et al., 2013). Furthermore, it has been proposed that inhibition is not covalent.

A recent study of our group described the first ever molecular docking studies of several 4-hydroxycoumarins into the active site of homology-modeled rat VKORC1 (Mladenović et al., 2012). The conformational analysis singled out Cys135 as a catalytic amino acid during the interaction of anticoagulants with the receptor. It was also maintained that hydrogen bonds and electrostatic interactions formed between polar groups of C-3 residues of active compounds and amino acids Thr138 and Tyr139 from the catalytic site of VKORC1 can significantly contribute to binding of anticoagulants into the active site and thereby increase the activity.

Performing similar molecular docking, we investigated the binding of **2f** and **2a** by two proposed mechanisms, non-covalent and covalent, respectively. The investigated compounds were docked into the active site of rat VKORC1 using the described methodology (Mladenović et al., 2012). When considering the mechanism of action, we proceeded from the fact that inhibition of the coagulation cycle occurs on reduced (activated) VKORC1. Afterwards, we investigated the mode of binding of our compounds to VKORC1 by means of irreversible or reversible inhibition.

*3.5.1. The binding mode of **2f** and **2a** according to the proposed non-covalent mechanism*

In the best-docked conformation of **2f**, the carbonyl group of the lactone part of the first chroman-2,4-dione ring is oriented towards the formation of a weak hydrogen bond ($d_{HB}$ = 3.178 Å) with the N atom of the Thr138–Tyr139 peptide bond (Fig. 3a). The chroman-2,4-dione ring itself is positioned towards Tyr139 by strong face-to-face hydrophobic π–π interactions between the ring and the Tyr139 phenyl group. The NH group of the Thr138–Tyr139 peptide bond additionally establishes important electrostatic interaction with the carbonyl group at position 4 of the second chroman-2,4-dione. A particular interaction greatly defines the conformation of **2f** within the active site, since its direct consequence is the arrangement of a second chroman-2,4-dione behind Tyr139. In that manner Tyr139 is encircled by **2f** in a sandwich-like conformation. The role of the ethylenediamine backbone in activity is to complete the spatial pocket around Tyr139 formed between the two chroman-2,4-dione cores and to additionally stabilize **2f** in the active site. Stabilization is accomplished because the amino group neighboring the second chroman-2,4-dione is narrow enough for electrostatic interaction with the hydroxyl group oxygen of Tyr139. Furthermore, attractive interactions mediate between the lactone carbonyl of the second chroman-2,4-dione and the SH group of Cys135. The latter interaction indirectly ensures proper orientation of the first C-4 carbonyl group of **2f** towards the amino acid hydrogen atom. Provided that the nature of interaction is a hydrogen bond, the SH group hydrogen atom can be easily transferred towards the C-4 carbonyl group of **2f** (Scheme 2), since the measured distance of the transfer path is $d_{HB}$ = 2.688 Å, inasmuch as hydrogen bonds are involved in proton transfer *via*

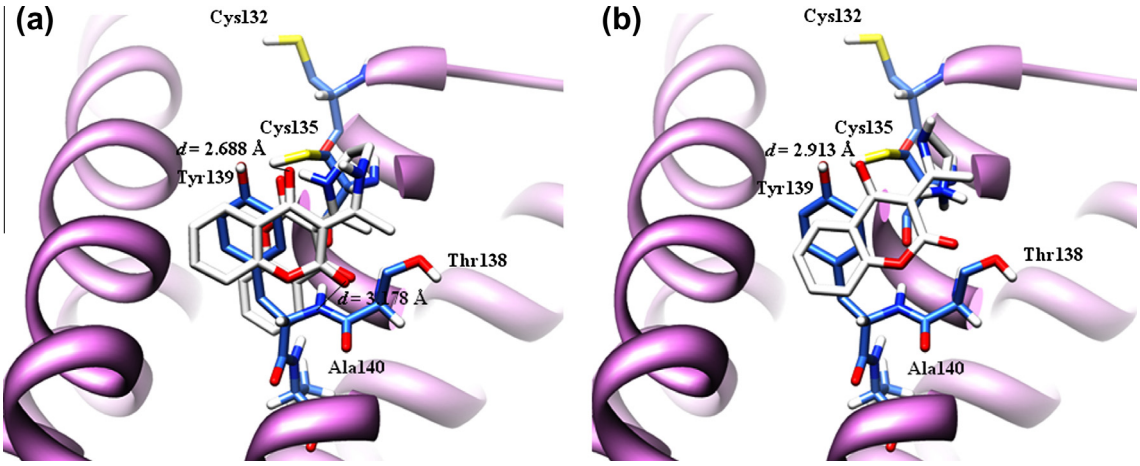


**Fig. 3.** Binding of the best-docked bioactive conformations of **2f** (a) and **2a** (b) into the active site of rat VKORC1 (to ensure clarity of the presentation, only polar hydrogen atoms are shown).

transition-state stabilization in enzyme catalysis (Schowen et al., 2000; Mladenovic et al., 2012). All of the quoted advantageous interactions of **2f** with the enzyme yield a low predicted K*i* value of 68.9 nM. Inhibition constants were predicted by the Lamarckian Genetic Algorithm and collected from the AutoDock output.

The spatial arrangement of **2a** (Fig. 3b) is comparable to that of **2f**. The position of the chroman-2,4-dione ring itself is quite similar to its position in **2f**. But despite the fact that the same interactions occur between Tyr139 and the molecule, it is in-plane rotated by approximately 30° in relation to the first chroman-2,4-dione ring of **2f** as a reference structure. Due to this rotation, there is no hydrogen bond with the Thr138–Tyr139 peptide bond, since the measured distance is $d$ = 4.112 Å. Inspection of the binding mode of **2a** further reveals several positive interactions. The protonated terminal amino group of ethylenediamine is narrowed to the hydroxyl group of Thr138, thus creating an electrostatic attraction. The C-4 carbonyl group is in suitable hydrogen-bonding orientation towards Cys135 ($d_{HB}$ = 2.913 Å). Since both **2a** and **2f** have a similar spatial arrangement within the active site, their anticoagulant activity should be comparable. This raises the following

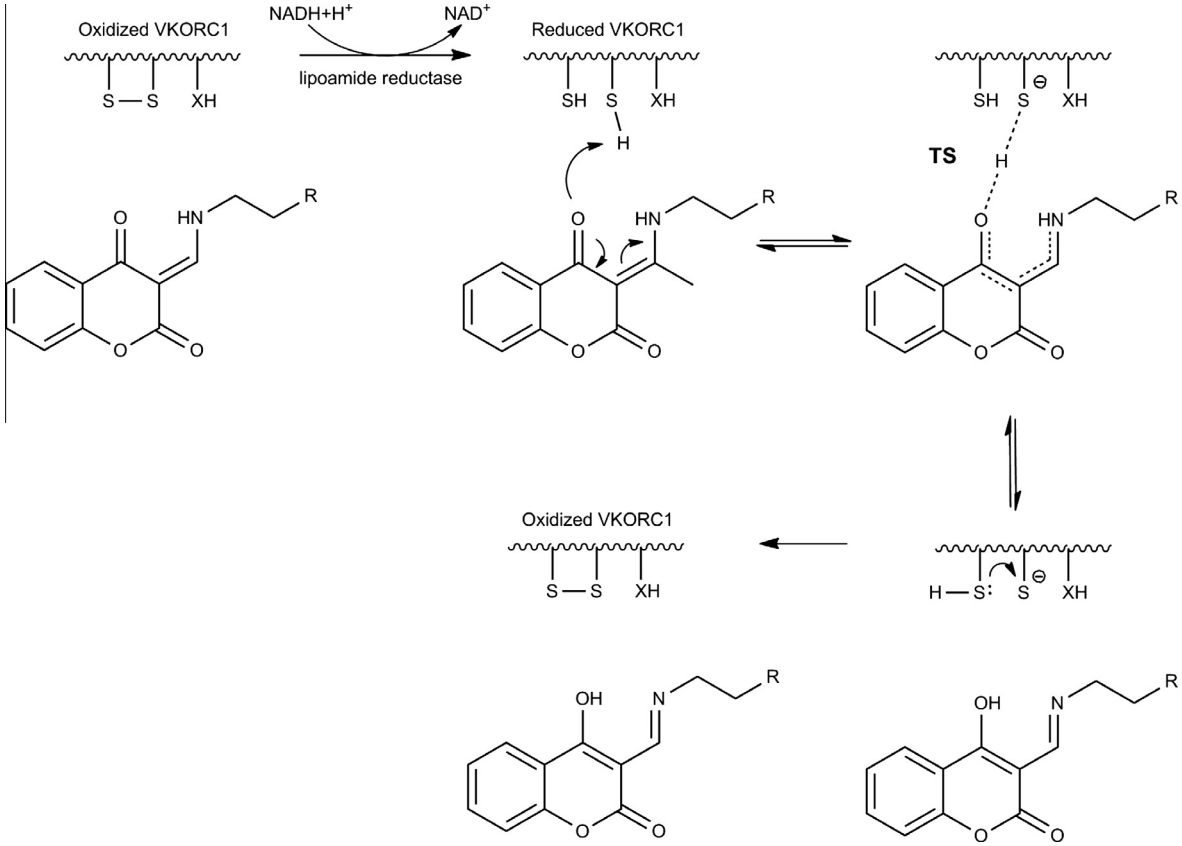


**Scheme 2.** Proposed mechanism for non-covalent inhibition of coagulation cycle by compounds **2a** and **2f**.

question: Why is **2f** more active than **2a**? A reasonable explanation is that the positioning of **2a** in the **2a**–VKORC1 complex in not as compact as the alignment of **2f** in the corresponding complex. For this reason, **2a** is not stabilized enough to easily accept a hydrogen atom from Cys135. The effect of the absence of strong binding is an estimated K*i* value of **2a** equal to 498.8 nM, which is lower than in **2f**.

The rest of the compounds showed significantly lower activity. Detailed structure-based explanations for the absence of the activity are presented in Supplementary information (Figs. S2–S4, and section *Molecular docking of non-active compounds*).

Based on all the presented findings and conclusions, Scheme 2 summarizes the probable mode of action of **2f** and **2a** *via* the non-covalent mechanism. Since Gebauer's work produced no conclusion about the mechanism of warfarin inhibition but only showed that the inhibition is reversible, our proposal for the mechanism is strictly structure-based, i.e., it is the result of understanding of the docking poses. The premise that the reaction is mediated by TS (transition state) is supported by the previous DFT mechanistic study (Mladenovic et al., 2012).

*3.5.2. Binding mode of **2f** and **2a** according to the proposed covalent mechanism*

When considering the covalent mechanism, it should be kept in mind that upon the VKORC1 initial reduction warfarin is (like vitamin K 2,3-epoxide) protonated by the active site, after which the unstable tautomer chroman-2,4-dione is formed (Silverman, 1980). This intermediate is susceptible to nucleophilic attack at the lactone carbonyl group when the VKORC1 active site is covalently modified by sulfhydryl acylation (pathway a) or acylation of the nearby nucleophile (pathway b). In the synthetic approach, the compounds evaluated in this study are chroman-2,4-dione derivatives that share structural similarities with vitamin K-2,3-epoxide and act as competitive inhibitors of VKORC1.

Compounds **2f** and **2a** can exert anticoagulant activity as irreversible inhibitors of VKORC1 (Scheme 3, according to Silverman, 1980) if the carbon atom of the lactone functional group undergoes nucleophilic attack by acylation with sulfhydryl of Cys135 (pathway a) or the hydroxyl group of Thr138 (pathway b).

The best-clustered docking pose of **2f** (Fig. 4a) represents a consequence of positioning of the second ring between Cys135 and Thr138, while the first ring is in comparison to the best-docked pose significantly relocated from Tyr139. Orientation of the second ring is influenced by electrostatic attraction between lactone oxygen and the hydroxyl group of Thr138. The carbonyl function at the C-4 position faces the Cys135 anion, but there are no electrostatic interactions. The measured distances between the compound and the active site amino acids suggest that there exists a possibility that the second ring can be a target for nucleophilic attack only *via* pathway b. The distance between the lactone carbonyl atom and Thr138 anion amounts to $d = 2.373$ Å, while the distance towards Cys135 anion equals $d = 5.743$ Å. On the other hand, relocation of the first ring caused values of the required distances to be elevated to values that cannot ensure covalent bonding, i.e., Cys135 and Tyr138 are too far away from the corresponding lactone carbonyl ($d = 7.108$ Å and $d = 7.643$ Å, respectively). The high value of the compound's predicted inhibition constant (K*i* = 312 mM) is confirmation that the best-clustered pose of **2f** is not the bioactive one.

The chroman-2,4-dione ring of **2a** (Fig. 4b) is in an almost orthogonal position with respect to Tyr139, a situation that leads to electrostatic attraction between the amino acid hydroxyl group and the lactone carbonyl of the chroman core. Additional stabilization is achieved by the fact that there is π–π electron interference between Tyr139 and the double bond of the C-3 residue. The lactone functional group is oriented towards the exterior, facing the membrane region. The protonated terminal amino group of ethylenediamine is narrowed to the phenyl ring of Tyr139, thus creating hydrophobic interactions. The measured distances between the lactone carbonyl atom and Cys132 or Thr138 anions are $d = 6.805$ Å and $d = 6.397$ Å, suggesting that there is no possibility of covalent bonding. In addition, the predicted inhibition constant of best-clustered **2a** is equal to K*i* = 819 mM.

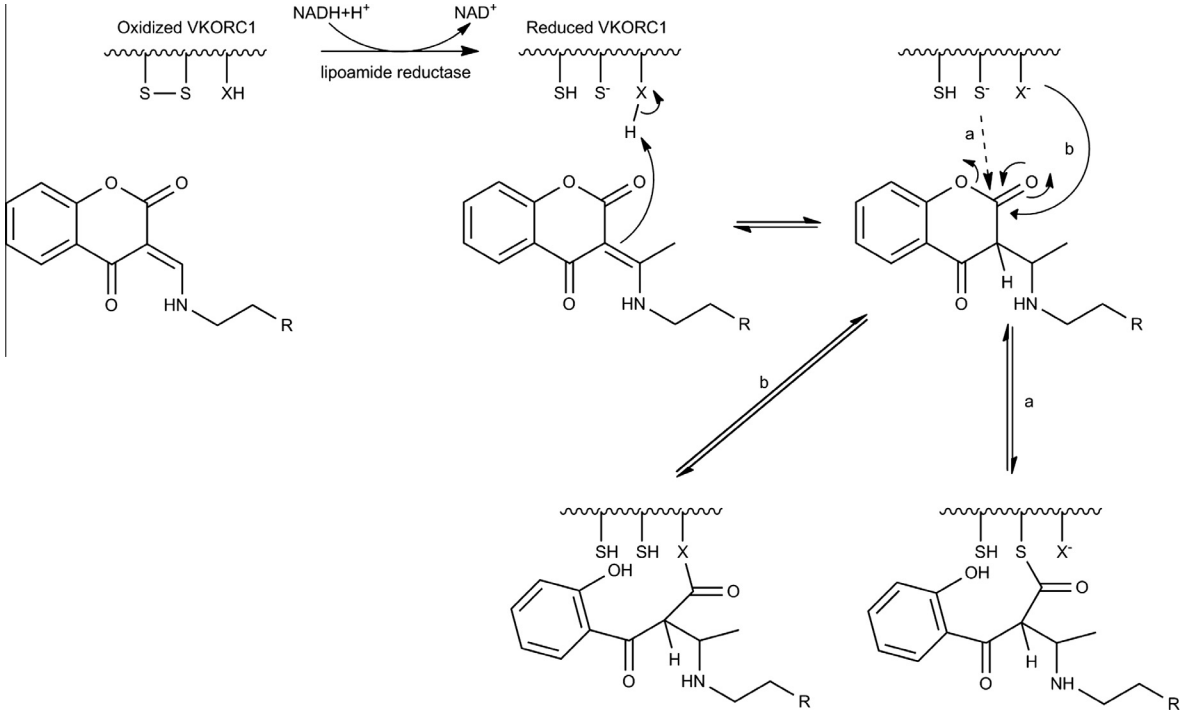


**Scheme 3.** Proposed mechanism for covalent inhibition of coagulation cycle.

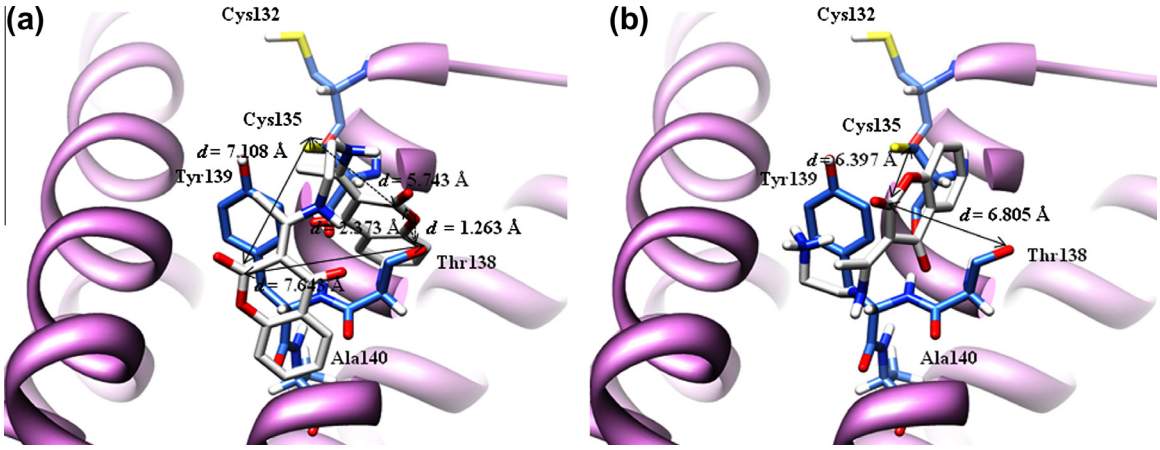


**Fig. 4.** Binding of best-clustered bioactive conformations of **2f** (a) and **2a** (b) into the active site of rat VKORC1 (for the sake of clarity, only polar hydrogen atoms are shown, the distances between the first ring and Cys35 and Thr138 being presented by a full line, while the corresponding distances with the second ring are depicted by a dashed line).

There is no consistency between the best-cluster poses of the tested compounds. It can therefore be concluded that the expression of anticoagulant activity by covalent binding to VKORC1 is difficult to achieve even for **2f**, despite the fact that there is an advantageous spatial alignment of the compound.

### 3.6. Pharmacophore modeling

The docking studies were further validated by the generation of meaningful 3-D pharmacophore models. A 3-D pharmacophore represents the relative position of important binding groups in space and disregards the molecular skeleton that holds them there (Patrick, 2009). Thus, the 3-D pharmacophore for a particular binding site should be common to all the various ligands which bind to it. Once the 3-D pharmacophore has been identified, structures can be analyzed to see whether they can adopt a stable conformation that will contain the required pharmacophore. If they do, and there are no steric clashes with the binding site, the structure should be active.

Qualitative HipHop models (Sakkiah et al., 2010) (Table S1, Supplementary information) were generated based on the best-docked alignment of the training set within the active site of VKORC1. Their purpose was to identify the crucial chemical features necessary for potent compounds and thereby provide some information for quantitative pharmacophore modeling. Compound **2f** was considered to be the reference compound. Fig. 5 presents the mapping of the best pharmacophore model onto **2f** and **2a**. For the sake of clarity, even hydrogen donor features related to Cys135 and Thr138 are depicted. The best HipHop hypothesis, *Hypo1*, shown in Fig. 5a, exhibits four features: two hydrogen-bond acceptors (HBA) and two hydrophobic aromatics (Hy), implying that these features are necessary and important for potent VKORC1 inhibition. The top 10 hypotheses and statistical parameters are given in Table S1 (Supplementary information).

In keeping with the information provided by *Hypo1* in qualitative pharmacophore modeling (Fig. 5a and b), the obtained chemical features were chosen as the initial ones in quantification of the model. Thus, the best quantitative hypothesis *HypoGen* (Fig. 5c and d, Table S1, Supplementary information) is characterized by the lowest total cost value (77.38), the highest cost difference (56.06), the lowest RMSD (0.71), and the best correlation coefficient (0.97). The fixed cost and null cost are 77.38 and 133.42 bits. All these parameters indicate that *Hypo1* has 75–90% probability of accurately predicting activity of compounds in the training set

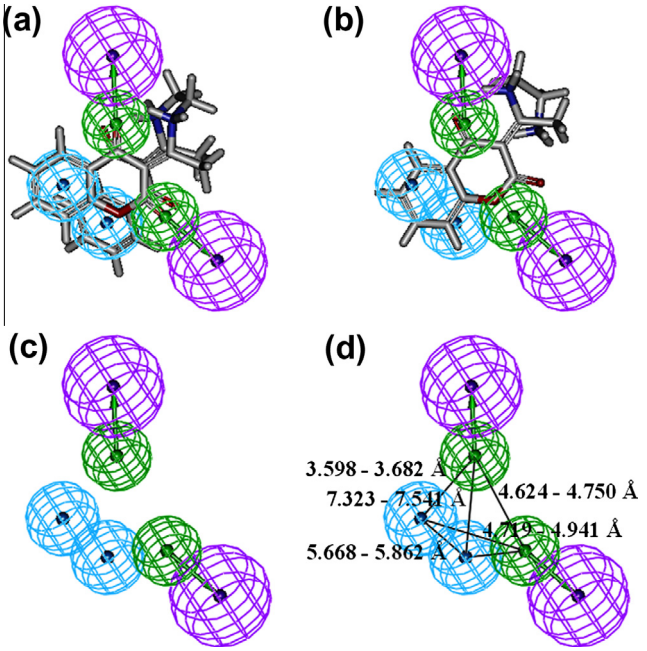


**Fig. 5.** The best pharmacophore model *Hypo1* aligned to **2f** (a) and **2a** (b), the HypoGen pharmacophore model of *Hypo1* (c), and 3-D spatial relationship and geometric parameters of *Hypo1* (d). Pharmacophoric features are color coded: green – hydrogen-bond acceptor; magenta – hydrogen-bond donor; blue: hydrophobic aromatic. (For interpretation of the references to color in this figure legend, the reader is referred to the web version of this article.)

(Table 4). The above validation confirmed that the *Hypo1* hypothesis was not derived by chance.

Used to further describe anticoagulant activity of the tested compounds, the generated structure-based pharmacophore models confirmed all significant interactions established in the compound–VKORC1 interaction mode. The best pharmacophore hypothesis consisted of a series of volumes related to hydrophobic aromatic (Hy) interactions, as well as hydrogen-bond acceptor (HBA) and hydrogen-bond donor (HBD) features. The Hy interactions (Fig. 5a and b, blue spheres) are crucial pharmacophore features of **2f** and **2a** and are a consequence of stabilizations between aromatic scaffolds of compounds and Tyr139. Moreover, the **2f** mode of action is characterized by two hydrogen-bond acceptor (HBA, green spheres) features located on the 4-carbonyl

**Table 4**
Actual and estimated activities of the training set molecules based on the phramacophore model *Hypo1*.

| Comp. | Fit value | $EC_{200}$ | Exp. $pEC_{200}$[a] | Pred. $pEC_{200}$[b] | Error[c] | Exp. scale[d] | Pred. scale[e] |
|---|---|---|---|---|---|---|---|
| **2a** | 7.46 | 3.98 | 2.40 | 2.41 | +0.01 | +++ | +++ |
| **2b** | 3.31 | 4.18 | 2.38 | 2.36 | −0.02 | ++ | ++ |
| **2c** | 5.44 | 4.23 | 2.37 | 2.34 | −0.03 | ++ | ++ |
| **2d** | 3.72 | 5.43 | 2.26 | 2.35 | +0.09 | ++ | ++ |
| **2e** | 4.12 | 8.93 | 2.05 | 2.22 | +0.17 | + | + |
| **2f** | 8.12 | 3.88 | 2.41 | 2.42 | +0.01 | +++ | +++ |
| **2g** | 3.92 | 3.31 | 2.48 | 2.53 | +0.05 | + | + |
| **2h** | 4.12 | 6.06 | 2.22 | 2.27 | +0.05 | + | + |

[a] Fit value indicates how well the features in the pharmacophore overlap the chemical features in the molecule. Fit = weight × [max (0.1 − SSE)] where SSE = $(D/T)^2$, $D$ = displacement of the feature from the center of the location constraints and $T$ = the radius of the location constraint sphere for the feature (tolerance).
[b] Exp. $pEC_{200}$ – experimental activity.
[c] Pred. $pEC_{200}$ – predicted activity.
[d] Error – Difference between the experimental and predicted activity: + values indicates that the predicted $pEC_{200}$ is higher than the experimental $pEC_{200}$; − values indicates that the predicted $pEC_{200}$ is lower than the experimental $pEC_{200}$.
[e] Activity scale – $pEC_{200} < 2.22$ = + (low active); $2.22 < pEC_{200} < 2.40$ = ++ (moderately active); $pEC_{200} > 2.40$ = +++ (highly active).

group and lactone oxygen from the pyrone moiety (Fig. 5a). The prediction of those properties highlights the extreme importance of the ability of the first **2f** chroman ring to accept the proton from Cys135 on the one hand, and the availability of a lactone carbonyl to accept the hydrogen bond for Thr138 on the other. Compound **2a** (Fig. 5b) is well aligned into *Hypo1* and shares two crucial features with **2f**: hydrophobic interaction with Tyr138 and the desired proton transfer from Cys135.

The *Hypo1* model was used to estimate inhibitory activities of the eight training set compounds. Table 4 shows experimental and estimated $pEC_{200}$ values of the entire training set. Clearly, $pEC_{200}$ values were correctly predicted, indicating that *Hypo1* is a good pharmacophore model.

### 3.7. Validation of pharmacophore model

The 3-D pharmacophore model derived from the excellent structure-based alignment was further used to predict activity of the test set. *Hypo1* was regressed against the 16 test set compounds, which gave a correlation coefficient of 0.810 between experimental and estimated activities. The results are presented in Fig. 6 and Table S2 (Supplementary information). It can be seen that *Hypo1* is well able to predict the activities of a wide variety of rat VKORC1 inhibitors.

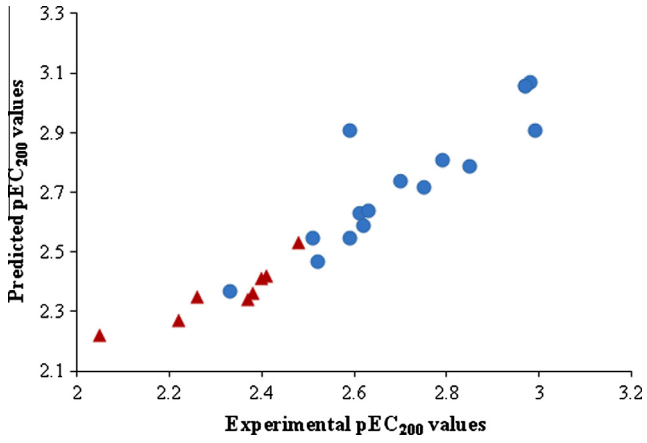


**Fig. 6.** Correlation plot between experimental and predicted $pEC_{200}$ values of training (purple triangles) and test (green circles) set molecules derived by quantification of *Hypo1*. (For interpretation of the references to color in this figure legend, the reader is referred to the web version of this article.)

### 3.8. Prediction of ADMET properties

Every time a new compound with excellent activity is discovered, it is a question whether or not that compound can become a drug candidate, depending on its water solubility or other druggability properties. It is therefore necessary to predict the ADMET properties of the leading compounds before further investigation. Optimization of these properties during the early stage of drug discovery is crucial for reducing ADMET problems in the later stage of evaluation. In this paper, ADMET properties including intestinal absorption, aqueous solubility, blood–brain barrier (BBB) penetration, Cytochrome P450 2D6 enzyme inhibition, hepatotoxicity, plasma-protein binding (PPB), atom-based Log*P* (Alog*P*), and polar surface area (PSA) were calculated in Discovery Studio (Zhang et al., 2012) for the examined eight compounds.

According to the values presented in Table 5, all of the compounds except **2h** can be efficiently absorbed in the human intestine. As the most active compounds, **2f** and **2a** can be classified as water soluble. Compound **2a** is more likely to be bound to carrier proteins than **2f**. They penetrate the BBB barrier with medium ease. Since they do not inhibit the Cytochrome P450 2D6 enzyme, the compounds can readily undergo hydroxylation in the first phase of metabolism and will be excreted as glucuronides. Compounds **2f** and **2a** are non-toxic, which is in accordance with the already presented results.

**Table 5**
Predicted ADMET properties for examined anticoagulants.

| Comp. | ADMET parameter | | | | | | | |
|---|---|---|---|---|---|---|---|---|
| | IA[a] | S[b] | BBB[c] | CYTP2D6[d] | PPB[e] | AlogP98[f] | PSA[g] | H[h] |
| **2a** | 0 | 3 | 2 | 0 | 2 | −0.753 | 88.595 | 0 |
| **2b** | 0 | 4 | 3 | 1 | 2 | 0.541 | 77.171 | 1 |
| **2c** | 0 | 3 | 3 | 0 | 2 | 1.513 | 56.341 | 0 |
| **2d** | 0 | 4 | 3 | 0 | 2 | −0.547 | 56.341 | 0 |
| **2e** | 0 | 3 | 2 | 0 | 0 | 2.226 | 112.683 | 0 |
| **2f** | 0 | 3 | 2 | 0 | 1 | 2.164 | 112.683 | 0 |
| **2g** | 0 | 3 | 4 | 0 | 2 | −0.204 | 120.998 | 0 |
| **2h** | 3 | 3 | 4 | 0 | 1 | 1.996 | 151.341 | 1 |

[a] Intestinal absorption (0: good, 1: moderate; 2: poor; 3: very poor).
[b] Solubility level (0: extremely low; 1: no, very low, but possible; 2: yes, very low; 3: yes, good; 4: yes, optimal; 5: no, too soluble).
[c] Blood–brain barrier penetration (0: very high; 1: high; 2: medium; 3: low; 4: undefined).
[d] Cytochrome P450 2D6 enzyme inhibition (0: non-inhibitor; 1: inhibitor).
[e] Plasma-protein binding (0: <90%; 1: >90%; 2: >95%).
[f] Atom-based Log*P* ($\leqslant -2.0$ or $\geqslant 7.0$: very low absorption).
[g] Polar surface area (>150: very low absorption).
[h] Hepatotoxicity (0: non-toxic; 1: toxic).

## 4. Conclusions

In evaluation of the *in vivo* anticoagulant activity of compounds **2a**–**h**, two of them, **2f**, and **2a**, presented high activity in concentration of 2 mg/kg of body weight. The prothrombin times of **2f** and **2a** were 130 and 90 s, respectively. Biochemical screening of serum and liver samples showed that the compounds do not cause hepatocyte necrosis and oxidative stress, which was also confirmed by histopathological studies. Molecular docking of compounds into the rat VKORC1 active site provided insight into the structural aspects required for activity and indicated a non-covalent mechanism of action. All important chemical features were confirmed in the generated structure-based 3-D pharmacophore model. The chroman-2,4-dione rings of both **2f** and **2a** are attracted by Tyr139 through strong hydrophobic interactions. More compact binding of **2f** into the active site is attributed to the formation of a spatial pocket around Tyr139 between the two chroman-2,4-dione cores as a consequence of ethylenediamine backbone conformation. The described hydrophobic attractions were characterized in terms of Hy chemical features. Upon reversible binding, Cys135 releases a thiol group proton towards the 4-carbonyl group of the first chroman-2,4-dione ring of **2f** and to the corresponding 4-carbonyl group of **2a**, which was confirmed by HBA 3-D pharmacophore spheres. According to computational ADMET evaluation, **2f** and **2a** are drug-like compounds.

## Acknowledgments

This work was financed by the Ministry of Education, Science, and Technological Development, Government of the Republic of Serbia, Grants No. III 43004, III 41010, and OI 173020. The authors would like to thank Professor Rino Ragno and Dr. Flavio Ballante, Rome Center for Molecular Design (RCMD), Dipartimento di Chimica e Tecnologie del Farmaco, Facoltà di Farmacia e Medicina, Università degli Studi Sapienza, Roma, Italia, for kind suggestions that have improved the computational procedures used in this work.

## Appendix A. Supplementary material

Supplementary data associated with this article can be found, in the online version, at http://dx.doi.org/10.1016/j.ejps.2014.01.004.

## References

Accelrys Software Inc., 2012. Discovery Studio Modeling Environment, Release 3.5. Accelrys Software Inc., San Diego.
Aitken, R.J., Harkiss, D., Buckingham, D.W., 1993. Analysis of lipid peroxidation mechanisms in human spermatozoa. Mol. Rep. Dev. 35, 302–315.
Au, N., Rettie, A.E., 2008. Pharmacogenomics of 4-hydroxycoumarin anticoagulants. Drug Metab. Rev. 40, 355–375.
Bergmeyer, H.U., Bowers, G.N., Hørder, M., Moss, D.W., 1976. Provisional recommendations on IFCC Methods for the measurement of catalytic concentrations of enzymes. Part 2. IFCC method for aspartat aminotransferase. Clin. Chim. Acta 70, 19–42.
Bergmeyer, H.U., Hørder, M., 1980. IFCC methods for measurement of catalytic concentrations of enzymes. Clin. Chim. Acta 105, 147–172.
Bevans, C.G., Krettler, C., Reinhart, C., Tran, H., Koßmann, K., Watzka, M., Oldenburg, J., 2013. Determination of the warfarin inhibition constant $K_i$ for vitamin K 2,3-epoxide reductase complex subunit-1 (VKORC1) using an *in vitro* DTT-driven assay. Biochim. Biophys. Acta 1830, 202–4210.
Bhatia, M.S., Ingale, K.B., Choudhari, P.B., Bhatia, N.M., Sawant, R.L., 2009. Application of quantum and physico chemical molecular descriptors utilizing principal components to study mode of anticoagulant activity of pyridyl chromen-2-one derivatives. Bioorg. Med. Chem. 17, 1654–1662.
Budzisz, E., Brzezinska, E., Krajewska, U., Rozalski, M., 2003. Cytotoxic effects, alkylating properties and molecular modelling of coumarin derivatives and their phosphonic analogues. Eur. J. Med. Chem. 38, 597–603.
Case, D.A., Darden, T.A., Cheatham III, T.E., Simmerling, C.L., Wang, J., Duke, R.E., Luo, R., Merz, K.M., Pearlman, D.A., Crowley, M., Walker, R.C., Zhang, W., Wang, B., Hayik, S., Roitberg, A., Seabra, G., Wong, K.F., Paesani, F., Wu, X., Brozell, S., Tsui, V., Gohlke, H., Yang, L., Tan, C., Mongan, J., Hornak, V., Cui, G., Beroza, P., Mathews, D.H., Schafmeister, C., Ross, W.S., Kollman, P.A., 2006. AMBER 9. University of California, San Francisco.
Coakes, S.J., Steed, L., Dzidic, P., 2006. SPSS Version 13.0 for Windows: Analysis without Anguish. John Wiley & Sons, Milton, Qld, Australia.
Deerfield II, D.E., Davis, C.H., Wymore, T., Stafford, D.W., Pedesen, L.G., 2006. Quantum chemical study of the mechanism of action of vitamin K epoxide reductase (VKOR). Int. J. Quantum Chem. 106, 2944–2952.
Ellman, G.L., 1959. Tissue sulfhydryl groups. Arch. Biochem. Biophys. 82, 70–77.
Fang, M.C., Go, A.S., Chang, Y., Borowsky, L.H., Pomernacki, N.K., Udaltsova, N., Singer, D.E., 2011. A new risk scheme to predict warfarin-associated hemorrhage: The ATRIA (anticoagulation and risk factors in atrial fibrillation) study. J. Am. Coll. Cardiol. 58, 395–401.
Fasco, M.J., Principe, L.M., 1982. R- and S-warfarin inhibition of vitamin K and vitamin K 2,3-epoxide reductase activities in the rat. J. Biol. Chem. 257, 4894–4901.
Fasco, M.J., Principe, L.M., Walsh, W.A., Friedman, P.A., 1983. Warfarin inhibition of vitamin K 2,3-epoxide reductase in rat liver microsomes. Biochemistry 22, 5655–5660.
Festa, G., Aglitti, T., Duranti, G., Ricordi, R., Perticone, P., Cozzi, R., 2001. Strong antioxidant activity of ellagic acid in mammalian cells in vitro revealed by comet assay. Anticancer Res. 21, 3903–3908.
Gebauer, M., 2007. Synthesis and structure–activity relationships of novel warfarin derivatives. Bioorg. Med. Chem. 15, 2414–2420.
Góth, L.A., 1991. A simple method for determination of serum catalase activity and revision of reference range. Clin. Chim. Acta 196, 143–152.
Henschel, H., Karlsson, B.C.G., Rosengren, A.M., Nicholls, I.A., 2010. The mechanistic basis for warfarin's structural diversity and implications for its bioavailability. J. Mol. Struct.: THEOCHEM 958, 7–9.
Hirch, J., Fuster, V., Aussel, J., Halpelin, J.L., 2003. American Heart Association/American College of Cardiology foundation guide to warfarin therapy. J. Am. Coll. Cardiol. 41, 1633–1652.
Jaffer, A., Bragg, L., 2003. Practical tips for warfarin dosing and monitoring. Cleveland Clin. J. Med. 70, 361–371.
Jendrassik, L., Gróf, P., 1938. Vereinfachte photometrische Methoden zur. Bestimmung des Blutbilirubins. Biochem. Zeitschrift. 297, 82–89.
Kaplan, M.M., Righetti, A., 1970. Induction of rat liver alkaline phosphatase: the mechanism of the serum elevation in bile duct obstruction. J. Clin. Invest. 49, 508–516.
Karali, N., Kocabalkanli, A., Gursoy, A., Ates, O., 2002. Synthesis and antitubercular activity of 4-(3-coumarinyl)-3-cyclohexyl-4-thiazolin-2-one benzylidenehydrazones. Il Farmaco 57, 589–593.
Karlsson, B.C.G., Rosengren, A.M., Andersson, P.O., Nicholls, I.A., 2007. The spectrophisycs of warfarin: implications for protein binding. J. Phys. Chem. B 111, 10520–10528.
Kataranovski, M., Živanović, J., Vranković, J., Mirkov, I., Kataranovski, D., 2007. Granulocyte-stimulating activity of the anticoagulant warfarin in rats. Arch. Biol. Sci. 59, 53–54.
Khoobi, M., Foroumadi, A., Emami, S., Savavi, M., Dehghan, G., Alizadeh, B.H., Ramazani, A., Ardestani, S.K., Shafiee, A., 2011. Coumarin-based bioactive compounds: facile synthesis and biological evaluation of coumarin-fused 1,4-thiazepines. Chem. Biol. Drug Des. 78, 580–586.
Killard, A.J., O'Kennedy, R., Bogan, D.P., 1996. Analysis of the glucuronidation of 7-hydroxycoumarin by HPLC. J. Pharm. Biomed. Anal. 14, 1585–1590.
Lassegue, B., Griendling, K.K., 2004. Reactive oxygen species in hypertension: an update. Am. J. Hypertens. 17, 852–860.
Lowry, O.H., Rosebrough, N.J., Farr, A.L., Randall, R.J., 1951. Protein measurement with the Folin phenol reagent. J. Biol. Chem. 193, 265–275.
Lukas, G., Brindle, S.D., Greengard, P., 1971. The route of absorption of intraperitoneally administered compounds. J. Pharmacol. Exp. Ther. 178, 562–566.
Małecka, M., Grabowski, S.J., Budzisz, E., 2004. Crystal and molecular structures of 3-[1-(2-hydroxyethylamino)-ethylidene]-chroman-2,4-dione and 2-methoxy-3-[1-(benzylamino)-ethylidene]-2,3-dihydro-2,4-dioxo-2k5-benzo[e][1,2]oxaphosphinane and DFT study of intramolecular H-bonds of related compounds. Chem. Phys. 297, 235–244.
Manokaran, S., Jaswanth, A., Sengottuvelu, S., Nandakumar, J., Duraisamy, R., Karthikeyan, D., Mallegaswari, R., 2008. Hepatoprotective activity of *Aerva lanata* Linn. against paracetamol induced hepatotoxicity in rats. Res. J. Pharm. Tech. 1, 398–401.
Marschall, H., Wagner, M., Zollner, G., Fickert, P., Diczfalusy, U., Gumhold, J., Silbert, D., Fuchsbichler, A., Benthin, L., Grundström, R., Gustafsson, U., Sahlin, S., Einarsson, C., Trauner, M., 2005. Complementary stimulation of hepatobiliary transport and detoxification systems by rifampicin and ursodeoxycholic acid in humans. Gastroenterology 129, 476–485.
MarwinSketch, ChemAxon, ChemAxon Kft.Záhony u. 7, Building HX 1031 Budapest, Hungary. <http://www.chemaxon.com>.
McIntosh, L.J., Trush, M.A., Tronsoco, J.C., 1997. Increased susceptibility of Alzheimer's disease temporal cortex to oxygen free radical-mediated processes. Free. Rad. Biol. Med. 23, 183–190.
Mihailović, V., Mihailović, M., Uskoković, A., Arambašić, J., Mišić, D., Stanković, V., Katanić, J., Mladenović, M., Solujić, S., Matić, S., 2013. Hepatoprotective effects of *Gentiana asclepiadea* L. extracts against carbon tetrachloride induced liver injury in rats. Food Chem. Toxicol. 52, 83–90.

Milton, N.G.N., 2008. Homocysteine inhibits hydrogen peroxide breakdown by catalase. Open Enzyme Inhib. J. 1, 34–41.
Mladenović, M., Mihailović, M., Bogojević, D., Vuković, N., Sukdolak, S., Matić, S., Nićiforović, N., Mihailović, V., Mašković, P., Vrvić, M.M., Solujić, S., 2012. Biochemical and pharmacological evaluation of 4-hydroxychromen-2-ones bearing polar C-3 substituents as anticoagulants. Eur. J. Med. Chem. 54, 144–158.
Mohamadi, F., Richards, N., Guida, W., Liskamp, R., Lipton, M., Caulfield, C., Chang, G., Hendrikson, T., Still, W., 1990. Macromodel—an integrated software system for modeling organic and bioorganic molecules using molecular mechanics. J. Comput. Chem. 11, 440–467.
Morris, M.G., Goodsell, S.D., Huey, R., Olson, J.A., 1996. Distributed automated docking of flexible ligands to proteins: parallel applications of AutoDock 2.4. J. Comput. Aid. Mol. Des. 10, 293–304.
Nalpas, B., Vassault, A., Charpin, S., Lacour, B., Berthelot, P., 1986. Serum mitochondrial aspartate aminotransferase as a marker of chronic alcoholism: diagnostic value and interpretation in a liver unit. Hepatology 6, 608–614.
Natala, S.R., Mallireddigari, M.R., Cosenza, S., Gumireddy, K., Bell, S.C., Reddy, E.P., Reddy, M.V.R., 2004. Synthesis of new coumarin 3-(*N*-aryl) sulfonamides and their anticancer activity. Bioorg. Med. Chem. Lett. 14, 4093–4097.
Ohkawa, H., Ohishi, N., Yagi, K., 1979. Assay for lipid peroxides in animal tissues by thiobarbituric acid reaction. Anal. Biochem. 95, 351–358.
Oldenburg, J., Marinova, M., Müller-Reible, C., Watzka, M., 2008. The vitamin K cycle. Vitam. Horm. 78, 35–62.
Oldenburg, J., Watzka, M., Rost, S., Muller, C.R., 2007. VKORC1: molecular target of coumarins. J. Thromb. Haemost. 5 (s1), 1–6.
Origin Pro 8, 2009. OriginLab Corporation, One Roundhouse Plaza, Northampton, MA, USA.
Patrick, G.L., 2009. An Introduction to Medicinal Chemistry, fourth ed. Oxford University Press, New York, USA.
Petitpas, L., Bhattacharya, A.A., Twine, S., Twine, M., East, M., Curry, S., 2001. Crystal structure analysis of warfarin binding to human serum albumin: anatomy of drug site I. J. Biol. Chem. 276, 22804–22809.
Pettersen, E.F., Goddard, T.D., Huang, C.C., Couch, G.S., Greenblatt, D.M., Meng, E.C., Ferrin, T.E., 2004. UCSF Chimera – a visualization system for exploratory research and analysis. J. Comput. Chem. 25, 1605–1612.
Quick, A.J., Stanley-Brown, M., Bancroft, F.W., 1935. A study of the coagulation defect in hemophilia and in jaundice. Am. J. Med. Sci. 190, 501–511.
Ragno, R., Simeoni, S., Rotili, D., Caroli, A., Botta, G., Brosch, G., Massa, S., Mai, A., 2008. Class II-selective histone deacetylase inhibitors. Part 2: alignment-independent GRIND 3-D QSAR, homology and docking studies. Eur. J. Med. Chem. 43, 621–632.
Ridker, P.M., Goldhaber, S.Z., Danielson, E., Rosenberg, Y., Eby, C.S., Deitcher, S.R., Cushman, M., Moli, S., Kessler, C.M., Eliot, C.G., Paulson, R., Wong, T., Bauer, K.A., Shwartz, B.A., Miletich, J.P., Baounameaux, H., Glyn, R.J., 2003. Long-term, low-intensity warfarin therapy for the prevention of recurrent venous thromboembolism. N. Engl. J. Med. 348, 1425–1434.
Rodríguez, S.A., Nazareno, M.A., Baumgartner, M.T., 2011. Effect of different C3-aryl substituents on the antioxidant activity of 4-hydroxycoumarin derivatives. Bioorg. Med. Chem. 19, 6233–6238.
Sakkiah, S., Thangapandian, S., John, S., Kwon, Y.J., Lee, K.W., 2010. 3D QSAR pharmacophore based virtual screening and molecular docking for identification of potential HSP90 inhibitors. Eur. J. Med. Chem. 45, 2132–2140.
Satyanarayan, V.S., Sreevani, P., Sivakumar, A., 2008. Synthesis and antimicrobial activity of new Schiff bases containing coumarin moiety and their spectral characterization. Arkivoc 17, 221–233.
Scholz, R.W., Graham, K.S., Gumpricht, E., Reddy, C.C., 1989. Mechanism of interaction of vitamin E and glutathione in the protection against membrane lipid peroxidation. Ann. NY Acad. Sci. 570, 514–517.
Schowen, K.B., Limbach, H.H., Denisov, G.S., Schowen, R.L., 2000. Hydrogen bonds and proton transfer in general-catalytic transition-state stabilization in enzyme catalysis. Biochim. Biophys. Acta 1458, 43–62.
Silverman, R.B., 1980. A model for a molecular mechanism of anticoagulant activity of 3-substituted 4-hydroxycoumarins. J. Am. Chem. Soc. 102, 5421–5423.
Silverman, R.B., 1981. Chemical model studies for the mechanism of vitamin K epoxide reductase. J. Am. Chem. Soc. 103, 5939–5941.
Singh, N.P., 2000. Microgels for estimation of DNA strand breaks, DNA protein crosslinks and apoptosis. Mutat. Res. 455, 111–127.
Software Spartan 2006 for Windows, 2006. Wavefunction, Inc., USA.
Sugiyama, T., Takaki, T., Sakanaka, K., Sadamaru, H., Mori, K., Kato, Y., Taguchi, T., Saito, T., 2007. Warfarin-induced impairment of cortical bone material quality and compensatory adaptation of cortical bone structure to mechanical stimuli. J. Endocrinol. 194, 213–222.
Sukdolak, S., Solujic, S., Manojlovic, N., Krstic, L.j., 2005. Synthesis and antimicrobial activity of new-[4-(4-Hydroxy-2-oxo-2-chromen-3-yl)thiazol-2-yl]benzenesulfonamides. Chem. Pap. 59, 37–40.
Tennant, B.C., 1999. Assessment of hepatic function. In: Loeb, W.F., Quimby, F.W. (Eds.), The Clinical Chemistry of Laboratory Animals, second ed. Taylor and Francis, Philadelphia, USA.
Thijssen, H.H., Janssen, Y.P., Vervoort, L.T., 1994. Microsomal lipoamide reductase provides vitamin K epoxide reductase with reducing equivalents. Biochem. J. 297, 277–280.
Tie, J.K., Stafford, D.W., 2007. Structure and function of vitamin K epoxide reductase. Vitam. Horm. 78, 103–130.
Walters, M.I., Gerarde, H.W., 1970. An ultramicromethod for the determination of conjugated and total bilirubin in serum or plasma. Microchem. J. 15, 231–243.
Wolber, G., Langer, T., 2005. LigandScout: 3-D pharmacophores derived from protein-bound ligands and their use as virtual screening filters. J. Chem. Inf. Model. 45, 160–169.
Zhang, Y., Liu, H., Jiao, Y., Yuan, H., Wang, F., Lu, S., Yao, S., Ke, Z., Tai, W., Jiang, Y., Chen, Y., Lu, T., 2012. De novo design of *N*-(pyridine-4-ylmethyl)aniline derivatives as KDR inhibitors: 3D QSAR, molecular fragment replacement, protein-ligand interaction fingerprint, and ADMET prediction. Mol. Divers. 16, 787–802.
Zhuo, X., Zhao, W., Zheng, J., Humhereys, W.G., Shu, Y.Z., Zhu, M., 2009. Bioactivation of coumarin in rat olfactory mucosal microsomes: detection of protein covalent binding and identification of reactive intermediates through analysis of glutathione adducts. Chem. Biol. Int. 181, 227–235.